universität wien

# MASTERARBEIT / MASTER'S THESIS

Titel der Masterarbeit / Title of the Master's Thesis

## First comparative study of afterpulsing behavior in single photon counting avalanche photo diode detectors


verfasst von / submitted by

Abdul Waris Ziarkash BSc


angestrebter akademischer Grad / in partial fulfilment of the requirements for the degree of

Master of Science (MSc)

Wien, 2017 / Vienna, 2017

| | |
|---|---|
| Studienkennzahl lt. Studienblatt / degree programme code as it appears on the student record sheet: | A 066 876 |
| Studienrichtung lt. Studienblatt / degree programme as it appears on the student record sheet: | Masterstudium Physik (UG2002) |
| Betreut von / Supervisor: | o.Uni.-Prof. Dr. Anton Zeilinger |

*Dedicated to my family*

# Abstract

Single-photon detectors, such as Avalanche Photo Diodes (APDs), have a great importance in many fields, including quantum key distribution, laser ranging, florescence microscopy, etc. Unfortunately APDs operated in Geiger mode, suffer from several non ideal behaviours of particular interest is the Afterpulse effect. Afterpulsing has different implications, depending on the intended application of the detector (fluorescence microscopy, quantum key distribution, etc.). Afterpulses can affect any application which measures the number or timing of detection events. Especially in quantum key distribution system, afterpulsing can adversely affect security and hence part of the security analysis [1–3].

Several studies have tried to link the afterpulsing behaviour to fundamental semiconductor physics. However, most of these studies have conflicting results. Some studies link the behavior to the distribution of discrete energy levels, while others formulate laws assuming continuous/quasi-continuous energy levels. Other studies posit "deep levels" while still more are based on Arrhenius law. The above works are inconstant with each other and are fundamentally different with conflicting results. To resolve the conflicts raised by these works and analyze the universality of these various theoretical models, we compare different commercial products against the canonical models proposed by previous studies. We show that the different behaviour observed is better attributed to individual piece to piece variation rather than fundamental laws of semiconductors. This lack of universality of the standard mathematical models of afterpulsing indicates that these studies can no longer be considered as of importance for semiconductor physics.

Despite not being related to fundamental semiconductor physics, afterpulsing, continues to remain a very important field of study as it applies to a wide variety of precision measurements in quantum optics and other fields. We provide a complete study of the afterpulsing effect, methods to characterise as well as its never before reported dependence on parameters like repetition rate, number of incident photons as well as their position and polarization. Moreover, here I present the first experimental demonstration on the presence of higher order afterpulses. The presence of such higher order afterpulsing was first speculated in [4] but never reported. Further, to demonstrate that the "Dead time" is a misnomer because the detector is not completely dead/inactive instead it exhibits a reduced detection efficiency, we use the cross-correlation function to investigate the so called "Dead time" region of various detectors.

These findings should be of interest not only to photonics quantum processing community but also researchers using Avalanche Photo Diodes (APDs) in other applications.

# Deutsche Kurzfassung

Einzelphotonen-Detektoren wie Avalanche-Photodioden (APDs) spielen in vielen Bereichen der Physik eine wichtige Rolle, wie bei der Quantenschlüsselverteilung, optischen Abstandsmessung, Fluoreszenzmikroskopie usw. Bedauerlicherweise weisen Avalanche-Photodioden, die in Geiger-Modus betrieben werden, verschiedene Mängel auf, insbesondere der Afterpulse-Effekt. Afterpulse haben je Gebiet der Anwendung des Detektors (Quantenschlüsselverteilung, Fluoreszenzmikroskopie, usw.) unterschiedliche Konsequenzen. Afterpulse beeinflussen jede Messung bei der die Anzahl bzw. der Zeitpunkt der Detektion gemessen wird. Insbesondere beim Quantenschlüsselaustausch können die Afterpulse die Sicherheit und damit einen Teil der Sicherheitsanalyse beeinflussen [1–3]. Mehrere Studien haben versucht, das Verhalten der Afterpulse mit Hilfe der Halbleiterphysik zu erklären. Allerdings kamen die meisten dieser Studien zu widersprüchlichen Ergebnisse. Einige der Studien verknüpfen das Verhalten der Afterpulse mit diskrete Energieniveaus innerhalb der Halbleiter des Detektors, während andere Studien kontinuierliche bzw. quasi-kontinuierliche Energieniveaus basierend auf das Arrhenius - Gesetz vorschlagen. Die vorgeschlagenen theoretischen Modelle zur Beschreibung des Afterpulses stehen im Widerspruch und unterscheiden sich grundsätzlich voneinander. Um diese Modelle zu analysieren, vergleichen wir nicht nur die Modelle, sondern auch verschiedene Detektoren miteinander. Wir können zeigen, dass die Verteilung der Afterpulse in jedem der einzelnen Detektoren sich unterscheidet und man daraus kein allgemeingültiges Modell für all APDs herleiten kann. Hiermit wird auch beschäftigt, dass die standardmäßigen mathematischen Modelle basierend auf dem Halbleiter des Detektors nicht mehr als zutreffend angesehen werden kann.

Nichtsdestotrotz, bleiben die Afterpulse ein sehr wichtiges Studienfeld, insbesondere für Präzisionsmessungen in der Quantenoptik und andere Bereiche der Physik. In der vorliegenden Arbeit führen wir eine vollständige Untersuchung der Afterpulse und zeigen eine Methode sie zu charakterisieren. Zusätzlich präsentieren wie eine nie zuvor beobachtete Abhängigkeit der Afterpulse von der Laserpulsfrequenz, Anzahl der Photonen pro Laserpuls sowie die Polarisation des Laserstrahls.

Darüber hinaus präsentiere ich hier die erste experimentelle Demonstration der höheren Ordnung der Afterpulse. Zwar wurde über die Existenz der höheren Ordnung der Afterpulse in [4] spekuliert aber bis zum jetzigen Zeitpunkt nie gezeigt. Zusätzlich zeigen wir mit Hilfe der Kreuzkorrelationsfunktion, dass im Bereich der "Totzeit" des Detektors, er nicht vollständig inaktiv ist, sondern nur eine reduzierte Detektionseffizienz aufweist. Diese neue Erkenntnisse sollten nicht nur für die Quanten-Photonik Gemeinschaft von Interesse sein, sondern auch für alle Forschungsbereiche, die Avalanche Photodioden (APDs) verwenden.

# Contents

# List of Publications

Some of the results of this thesis have been reported in the following publication

1. **Abdul Waris Ziarkash**, Siddarth Koduru Joshi, Mario Stipčević and Rupert Ursin. "**First comparative study of afterpulsing behavior in single photon counting avalanche photo diode detectors.**" *Submitted to Optics Express.*

Contribution in following publication

2. Matthias Fink, Ana Rodriguez-Aramendia, Johannes Handsteiner, **Abdul Waris Ziarkash**, Fabian Steinlechner, Thomas Scheidl, Ivette Fuentes, Jacques Pienaar, Tim C. Ralph, and Rupert Ursin. "**Experimental test of photonic entanglement in accelerated reference frames.**" *Accepted for publication in Nature Communications.*

# List of Patents

"**Characterization of afterpulses in a single photon detector**". *Patent pending.*

# List of Figures

# List of Tables

# Definitions of some terms

**Quantum Efficiency $\eta_{\mathbf{QE}}$**

Quantum efficiency $\eta_{\mathrm{QE}}$ is the conversion ratio of an absorbed photon into an photo-electron and does not include the varies physical phenomena like (absorption, etc) that results into overall detection efficiency. Sometimes quantum efficiency $\eta_{\mathrm{QE}}$ of a detector is used as synonymic to its detection efficiency $\eta_{\mathrm{DE}}$. This is *not* the same as detection efficiency.

**Active Area**

The active area is defined as the absorbing region of a detector.

**Photon Detection Efficiency $\eta_{\mathbf{DE}}$**

The detection efficiency $\eta_{\mathrm{DE}}$ is the overall probability that an incident photon is absorbed by the active area of the detector and also generates an electric output signal. For a photon to be detected, it is not enough to be absorbed by the detector that generates a primary electron-hole pair, but it is also necessary that the primary electron-hole pair succeeds in triggering an avalanche.

**Dark Counts**

Dark counts are additional counts not originating from incoming photons. Dark counts arise due to electrical and thermal noise. Furthermore, dark counts occur even in absence of an incident photons by randomly generated carriers traversing the depleted region, triggering an avalanche and producing output current pulses.

**Background Counts**

Background counts are not an intrinsic property of a detector, but due to stray light from external sources hitting/reaching the detector and causing spurious detection events. Depending on the sensitivity of the detectors for the mid- or far-infrared photons, some detector are more susceptible to it than others.

**Noise Counts**

The noise counts rate of a detector is the dark count rate plus the background count rate.

**Detected Photon Per Laser Pulse (DPPLP)**

In order to objectively compare afterpulsing data obtained from different detectors and correctly evaluate the effect of afterpulses in different fabrications, we define a key parameter (DPPLP). When an attenuated pulsed laser is incident on a single photon detector, the ratio of the number detection clicks to the number of pulses emitted by the laser is called DPPLP.

**Dead Time**

The so called dead time" ($t_{dead}$) is the period of time after the initial photon detection. During which the detector is recovering and resetting itself, so that it is incapable of processing any further detections. The dead time may be caused by intrinsic processes in the photosensitive system or it may be induced by external control systems in order to produce a particular performance characteristic [9].

**Twilighting**

The dead time of a detector is subject to statistical fluctuations, anomalies in these statistics have been termed twilighting.

# Chapter 1

# Introduction

Single photon detectors, like Avalanche Photo Diodes (APDs) are essential for many quantum optics experiments. Such detectors have been extensively studied over the past century. Unfortunately they suffer from many non ideal characteristics (non-unity quantum efficiency, dead-time, etc.). Including the generation of more than one electrical signal for each photon detection event called afterpulsing.

One of the initial models – the multiple exponential model – to characterize the afterpulse behaviour was proposed by Cova et al.. In 1991, Cova et al. investigated Silicon APDs to demonstrate the afterpulse effect and came upon that the afterpulsing effects can be evaluated by using the time-correlated carrier counting technique (TCCC). Since then, several previous works have attempted to characterize the afterpulse behavior and fit the results to various models such as the power model or hyperbolic sinc model [4, 13–18].

Worryingly, these works do not agree on the most suitable model describing the statistics of the arrival times. All these studies have focused on one make/manufacture of detector at a time. Furthermore, all of the studies to date used one specific laser pulse frequency, DPPLP values and laser beam polarization to investigate the afterpulse effect.

In this thesis I will present a complete study of afterpulse effects by performing the first comparative study of afterpulsing behavior in multiple single photon counting avalanche photo diode detectors. By comparing all the canonical models of afterpulsing I probe the causes of the contradictions between the previous works and show that none of the models applied are universal.

A comparison among individual detectors and several makes of detectors (SPCM-AQ4C from PerkinElmer, SPCM-NIR from Excelitas and $\tau$-SPAD-fast from Laser Components) are not enough to carry out a detailed analysis of afterpulsing effect; it is also necessary to take many parameters (e.g. Laser pulse frequency, DPPLP values and laser beam polarization) into account. This why I evaluated the afterpulsing effects by using various laser pulse frequency/polarization/DPPLP values.

Furthermore, I eschew the common practice of using auto-correlation function to use a novel technique – the so called cross-correlation – to characterize the afterpulsing behaviour. The cross-correlation gives all the information as auto-correlation and even more e.g. the timing correlation between the detector and photon source.

Yet, with the use of cross-correlation functions, it allows us an investigation of the behaviour during the dead time and check for high order afterpulses that was speculated in [4]. In this thesis I present the presence of higher order afterpulses, that has not been observed nor accounted for in any of the standard models of afterpulse behavior.

# Chapter 2

# Single photon detection

Single-photon detectors, like Avalanche Photo Diodes (APDs), have a great importance in many fields. Such as in photonics quantum processing tasks like quantum key distribution (QKD), laser ranging, fluorescence microscopy, neural imaging with blood flow tomography, contrast-enhanced MRI, two-photon luminescence imaging, astronomical telescopes, etc. [7, 19–24]. These applications of single-photon detectors focus on the timing of a very weak optical signal and the ability to detect very low light intensities, down to individual photon pairs.

Avalanche photo diodes are the most widely used single-photon detectors for visible and Near-infrared, but other class of detectors like Photo Multiplier Tubes (PMTs), Transition Edge Sensors (TES) or superconducting nanowire single-photon detector (SNSPD) APDs are also a common alternative. These semiconductor-based detectors Avalanche Photo Diods are not only a less demanding alternative to TES and SNSPD but also are an inexpensive alternative to PMTs. Besides the well-known advantages of solid state versus vacuum-tube devices (small size, ruggedness, low power dissipation, low supply voltage, high reliability, low cost, etc.), semiconductor detectors provide inherently higher detection efficiency (up to 60 %), particularly in the red and near-infrared spectral regions [9]. In this chapter I will present working principles of an the most common single photon detectors like APDs, PMTs, TES and SNSPDs with a emphasis on a typical non-ideal behavior of APDs known as afterpulsing.

Afterpulses lead to an overestimation of the total count rate by up to 10 % as well as a reduction of the duty cycle and detection efficiency due to the increased dead times. In quantum communication the overestimation of coincidence events leads to larger Quantum Bit Error Rate (QBER). Afterpulsing does not only affects any application which measures the number or timing of detection events, but can also adversely affect security [3] and hence part of the security analysis of the quantum key distribution system.

## 2.1 Photomultiplier tube

After the invention of the first single-photon detectors approximately 90 years ago, ever since it has been an active area of research and development. The semiconductor-based APDs are currently best suited class of detectors to applications such as photonics quantum processing tasks like quantum key distribution (QKD), laser ranging, fluorescence microscopy, etc. In order to aid with single detector selection and show the great importance of APDs in comparison to the other alternatives, we discuss the most common class of detectors.

Photo Multiplier Tube (PMT) became in the 1930 the first device to detect light at the single photon level. The detection of a single photon is based on the photoelectric effect and secondary emission. After an incident photon enters the vacuum tube by hitting (propagating through) the photocathode , it can knock out multiple electrons – these emitted electrons are called photoelectrons [9]. By applying an electric field the photonelectrons are accelerated to the first dynode to knock out even more electrons. In order to achieve a sufficient high enough current for the electronics of detector to be detectable, the process of acceleration and multiple electron emission process is repeated on subsequent dynodes. From the last dynode the secondary electrons are collected on the anode [7, 9, 25].

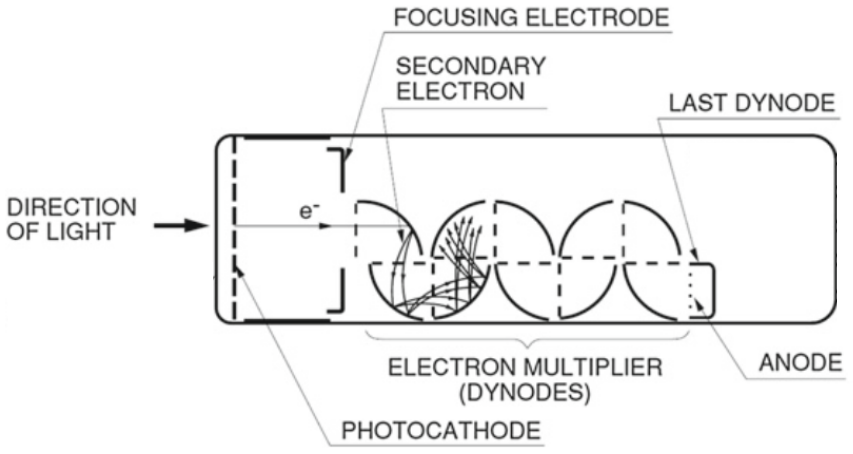


**Figure 2.1:** The working principle of a photomultiplier. After the photoelectron hitting the first dynode, we can observe the multiplication of secondary electrons on the subsequent dynodes (typically there are about 10 to 20 dynodes) inside a photomultiplier tube.

Due to its fast response (short dead time and low timing jitter) low dark count level and a large sensitive areas (up to a $m^2$ [7]) these single photon-counting technology invented nearly 90 years ago, is still use. In particular in nuclear physics or biological and medical applicantions (e.g. for blood analysis etc). Unfortunately, they are suffer from some major drawbacks such as large in size compared to APDs, a high-voltage supply, low detection efficiency (≈2 % at near IR), limited lifetime and afterpulses (≈3 % - 4 % total afterpulse probability [26]).

## 2.2 Transition edge sensors

The superconducting Transition-Edge Sensors (TES) operate as a bolometer, that can detect the thermal energy deposited by a single photon [5, 7]. In particular, the rise in temperature (caused by the absorption of an incident photon) is used to exploit the temperature-dependent resistance of the superconducting phase transition [6, 7, 9, 27].

The TES consists of three main components: an absorber, a sensitive thermometer and a weak thermal link to a cold bath to cool the detector [6, 9].Once an incident photon hits the absorber it heats up due to the incident energy and cooled down by the thermal link to base temperature to dissipate the absorbed energy.

In order to detect the energy of an individual photon, an extreme sensitivity is required. This employs an absorber with low heat capacity and an extreme sensitive thermometry with a large response to small temperature change [7, 9].

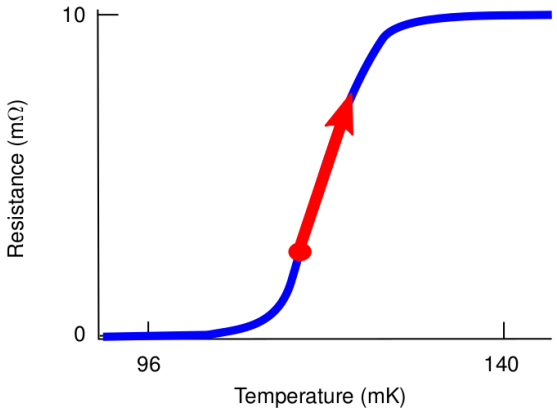


**Figure 2.2:** On this graph the strong resistance-temperature dependency of an superconducting is shown. Absorption of a single incident photon is sufficient to increase the temperature and therefore the resistance of the superconductor. The resultant current drop, which is amplified by the SQUID, is detectable for the electronic of the detector. Graph taken from [5].

To achieve such a sensitivity, a thermometer made from a superconducting film (usually made of tungsten) maintained near its critical temperature $T_c$ such that a slight change in temperature (due to the energy of an absorbed single photon) is sufficient to induce its transition from superconductor to normal resistance. A constant voltage bias is applied across the superconductor film, which increases the temperature of the electrons and maintained the device at this temperature through electro-thermal feedback [1] [7]. This means that when a photon is absorbed, the temperature increases, transition from superconducting to normal phase transition happens. This results in an increase of electrical resistance, which causes a drop in TES current, which reduces the Joule heating of the device. Using a sensitive current amplifier such as Superconducting Quantum Interference Device (SQUID), the small change in current flow can be detected [5, 7].

[1] A electro-thermal feedback is the interaction of the electric current and the temperature in a device with a temperature-dependent electrical resistance. This interaction arises from Joule heating.

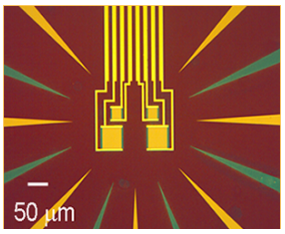


**Figure 2.3:** The active area of a transition edge sensors made of four tungsten superconductors. Graph taken from [6].

Unlike PMTs, APD and SNSPDs, these transition-edge sensors can distinguish between the number of incident photons simultaneously arriving based on the total amount of energy absorbed. Moreover, TES detectors have demonstrated detection efficiencies approaching unity ($\eta_{\mathrm{DE}}$ of $> 95\%$ at 1550 nm and $\eta_{\mathrm{DE}} > 98\%$ at 850 nm). It can detect radiation in many wavelength ranges (from sub-mm wavelengths to gamma-rays) and have negligible dark counts.

However, they suffer from some ill effects as compared to the APDs. There biggest weakness is the low operating temperature (it can can vary between devices from some tens up to some hundreds of mK). Another weaknesses of TES are the long recovery times, mostly limited by the thermal link. The recovery time to reset the detector is in the order of 1 - 2 $\mu$s, limiting the maximum count rate. TES also have a high timing jitter of ($\approx$ 50 ns to 100 ns [28]) compared to all other discussed detector types (see Table 2.1).

| Type of Detector | Wavelength range | Detection Efficiency | Dark counts (s-1) | Dead time | Jitter (ns) | Photon number resolving |
|---|---|---|---|---|---|---|
| PMT | 100 - 900 n | 8 - 28% | 1 - 200 | 1 $\mu$ s | $< 1$ | $\times$ |
| Si APD | 400 - 1100 nm | 20 - 60% | $\approx 50$ | 22 ns s | $< 1$ | $\times$ |
| TES | Visible, Near IR | $> 98$ % | $< 1$ | — | $\approx 100$ ns | $\surd$ |
| SNSPD | Visible, Near IR | $> 93$ % | $< 1$ | 40 ns | 0.1 | $\surd$ |

**Table 2.1:** A comparison between single photon detectors. The data were taken from [5, 7, 9] and also from our measurements.

## 2.3 Superconducting nanowire single-photon detectors

The Superconducting Nanowire Single-Photon Detector (SNSPD) are based on a current-biased superconducting nanowire [29]. These superconducting nanowires are biased with a current near the critical current, just below the value where the wires reverts from superconductive region to normal state (non-superconducting region) in response to the absorption of incident photons.

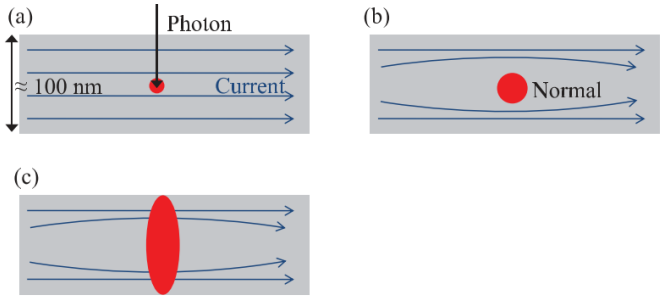


**Figure 2.4:** A schematic representation of absorption of a photon and the subsequent transition of a superconducting region into a non-superconductiong region (also called normal region). The superconducting nanowires used in SNSPDs are very thin ($\approx 5$ nm) and narrow ($\approx 100$ nm). Figure taken from [7].

The energy of the absorbed photon creates a hotspot – non-superconducting region (a nanoscopic length within the nanowire) – by reducing the local critical current and resulting in a finite electrical resistance in that spot. Due to the subsequent Joule heating as a results of current flowing through this now resistive region, it spans the full width of the nanowire (see Figure 2.4). As a consequence a measurable voltage pulse is yield that indicates the detection of an incoming single photon.

Like TES, SNSPDs have also a high detection efficiencies of $> 93\,\%$ for wavelength of visible and near IR light [5]. However in contrast to TES, SNSPDs have low timing jitter ($1\,\%$), high count rates and they do not suffer from afterpulsing effect. Nevertheless, their reliance on cryogen cooling systems (generally operated at ≈1K or even lower temperatures [9]) makes them expensive. Another disadvantages of SNSPDs are their small active area and polarization dependence [9, 30].

## 2.4 Avalanche photodiodes

An Avalanche Photo Diodes (APDs) are the backbone of single photon detection. These highly sensitive semiconductor electronic devices are operated above their breakdown voltage in "Geiger" mode. Like the first single photon detectors – Photo Multiplier Tubes (PMTs) – APDs are based on the photoelectric effect to convert optical signals (low energies of single photons ($\approx 10^{-19}$ J)) into electrical signals. APDs consisting of

a p-n junction serve as a detector and are able to detect a single photon with detection efficiencies of $\approx 50\,\%$ (at 810 nm).

### 2.4.1 Principles of Operation

Once an incident photon is absorbed in the N-region of semiconductor's PIN structure, it creates an electron-hole pair (an electron in the conduction band and a hole in the valence band). Under a strong enough electric field the electrons are accelerated towards the P-region, thereby increasing its energy with respect to the bottom of the conduction band. If the energy of the electron is greater than the band gap energy $E_g$[2], the electron can create new electron-hole pairs by means of impact ionization. Newly generated carriers are also accelerated under the effect of the field to produce further electron-hole pairs, and this process repeats itself. This results in an avalanche effect that produce a current that is sufficient to be detected by the electronics following the APD [31, 32].

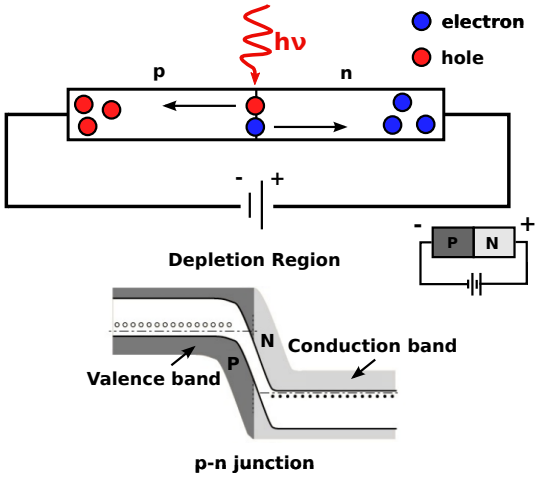


**Figure 2.5:** Reverse biased p-n junction, where no current can flows and a depletion layer between the both p and n-Region is created. Once an incident photon creates an electron hole pair in the depletion region, they are swept out of the region creating a current [8].

The APD's semiconductor's design has to fulfill two crucial requirements in order to efficiently perform this avalanche process. Besides maximizing the photon absorption, it has to minimize the possibility of localized uncontrolled avalanches being produced by the strong electric field [32]. A reverse-biased p-n junctions [3] is used in an usual avalanche photodiode (APD).

In order to understand the avalanche effect in a diode let us first look at a reversed biased PN junction. Applying reverse bias voltage to the diode, the electrons in the N-Region and electron-hole pairs at the P-Region will get pulled from junction region towards the terminals and the depletion region expands with an increase in the electric

[2] $E_g$ is the energy difference between conduction and valence band in Semiconductors.

[3] The p-n junction is operated by applying an external voltage – forward or reverse biased. A process called "biasing"

field strength. It appears as a parallel plate capacitor and ordinarily does not conduct. Thus preventing current from flowing through the semiconductor material [33, 34].

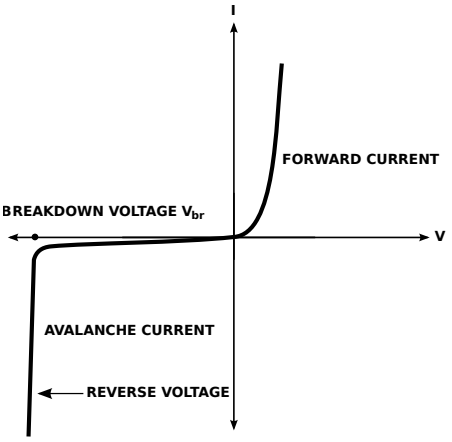


**Figure 2.6:** I-V characteristic curve of the p-n junction. In a p-n junction, there are three possible biasing conditions – Zero Bias, Reverse Bias and Forward Bias. Only the reverse bias is relevant for our purpose. In a Reverse Bias condition, a positive voltage is applied to the N-type material and a negative voltage is applied to the P-type material. It prevents a current flow through the diode. When exceeding the breakdown voltage $V_{br}$ the diode is shorted and it will result in the flow of maximum circuit current (avalanche current).

The most common practice is to operate these reverse biased APD's p-n junctions just above the breakdown voltage $V_{\mathrm{br}}$ to achieve a photon-counting operation of low intensity signals (down to the single photon). Detectors in this operating condition have been referred to as "Geiger" mode a avalanche photodiodes. This means that due to the high operating voltage (100 V to 300 V), absorbtion of a single incident photon (by the depletion region) leads to a complete breakdown of the diode by triggering the self-sustaining avalanche [35, 36].

The current then grows exponentially until the space-charge effect [4] limits it to a constant level. The p-n junction is thus switched to the "on" state, where a constant macroscopic avalanche current flows. The fast onset of the current marks the time of arrival of the photon that generated the initial charge carrier [9]. Since the avalanche is self-sustaining, the detector stays in this condition until resetting the bias voltage to the original level above breakdown. A external quenching circuit needs to be implemented in order to stop the avalanche and ensure the recovery of the APD as soon as possible [39]. The process of using an external circuit to reset the detector and bring it back to the original level above breakdown voltage is called quenching [40].

[4] Space-charge effect is the result of mutual repulsion of particles like charge (electrons, etc.) in the regions near the p-n interface and forming the space charge region or depletion layer (see Figure 2.5)[37, 38].

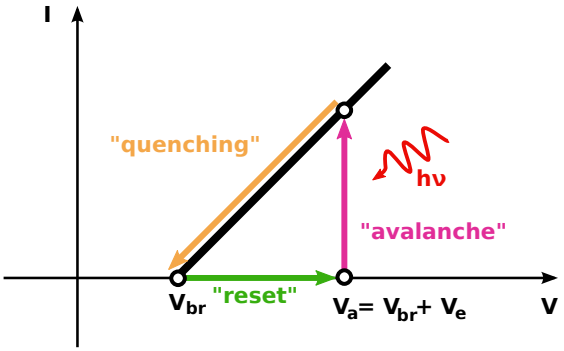


**Figure 2.7:** APD operation in the reverse I-V characteristics of a p-n junction. The device is biased at voltage $V_a$ above the breakdown voltage $V_{br}$. After an avalanche multiplication process the quenching circuit resets the voltage from the excess bias voltage $V_a$ to the original level above breakdown. Figure taken from [9]

### 2.4.2 Passive quenching

As mentioned in Section 2.4, once an avalanche process has been triggered, an external quenching circuit is required to reset the device. By lowering the bias voltage the breakdown voltage to the original level above breakdown, one prevents the avalanche process to take place. Then, the bias voltage is restored to detect another subsequent incident photon [10, 35, 41].

There are two ways to quench APDs, either passive or active. The quenching is main reason for the dead time of detectors. According to canonical understanding, during the quenching process the detector can not respond to any subsequent photon arriving while the bias voltage is restoring. However, using the cross correlation technique described in Section 3.1, we able to show the non zero probability of a count during the "dead-time" (see Section A).

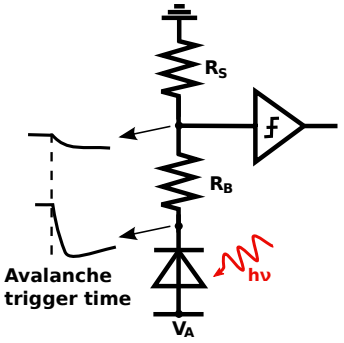


**Figure 2.8:** Schematic representation of a passive quenching circuit (PQC). $R_B$ is the high-value ballast resistor and $R_S$ the APD's series resistance [10].

The simplest way to operate an APD in the Geiger mode is quench a detector by using a passive quenching circuit (PQC). For passive quenching, the APD is placed in series with a high-value ballast resistor $R_B$. The resistor value, which varies (typical tens of $k\Omega$), depends on the capacitance of the junction and the desired response/dead time

of the circuit. On photo-detection the current raises by $V_e$ to the value of $V_a$. The current final value is given by the excess bias voltage $V_e$ (see Figure 2.7) divided by the ballast resistance $R_B$. This current discharges the parasitic capacitance $C_P$ at the APD cathode, so the excess voltage decreases exponentially towards zero [10]. This voltage drop across the resistor quenches the breakdown [40]and it can slowly recovers through the natural dead time and recharge itself to its initial bias level and is ready for the subsequent incident photon detection. The recharging time of the APD follows an exponential loading curve. Depending on the voltage, the value of the resistor used in the circuit, this loading characteristics can vary, however it lead to an effective dead time of about $\approx 1-2\,\mu$s, which limits the maximal count rate to to a few hundred thousand cps. [35, 36, 41].

### 2.4.3 Active quenching

From a historical perspective the initial idea of Active Quenching Circuits (AQCs) was first reported in 1975 [42]. In active quenching, the main idea is to overcome/improve on the slow passive quenching circuits (PQCs). One of the main problems of a PQC is that it has a slow and not very well defined recovery dead time. Therefore, to exploit fully the inherent potential of an APD, one requires an AQCs to reset the detector, with a controlled bias voltage, as quickly as possible after an occurrence of a detection event [10]. A large resistor used in passive quenching circuit is replaced with small resistor (few k$\Omega$) to stop the self-sustaining avalanche. Once the current through the resistor increases, which it does very rapidly, it gives a feedback to the system and then the active components (fast comparator and transistor) are used to switch the voltage across the APD below breakdown, so that after a well defined hold-off time, the bias voltage is set back to the operating level [43]. Unlike passive quenching the whole active quenching process is in the order of some picoseconds and due to an accurately controlled hold-off the dead time is well-defined.

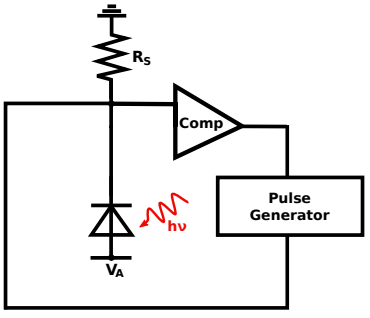


**Figure 2.9:** A basic diagram of an active quenched circuit (AQC). The rise of the avalanche pulse is sensed by the comparator, whose output resets the bias voltage to the breakdown voltage $V_{br}$ or below. After a fixed time, the bias voltage is switched to $V_A$ [10].

The actual performance of the avalanche photodiodes are drastically affected by the features of underlying quenching circuit used. Although passive quenched detectors are

attractive because they are simple, cost less, they inherently limit the average current in the detector device thus preventing excessive power dissipation and heating, and give easily detectable output pulses. The count rate is limited at $\approx 200$ kc/s, therefore passive quenched detector have a limited application [35].

On the other hand, the active quenched detectors are much faster than the passive quenched detectors, have a shorter dead times (few tens of nanoseconds in Si APDs) and achieve counting rates of up 30 Mc/s [7]. Unfortunately, these detectors suffer from a non ideal behaviour called afterpulsing. (A detailed analysis of this can be found in Section 2.5)

## 2.5 Afterpulses

In the past the afterpulsing behaviour has been linked to charges been trapped in the deep levels [5] of the semiconductors band structure. During each avalanche process, some carries may be trapped in these deep levels and subsequently released with a statistically fluctuating delay. A released carrier can re-trigger the avalanche process and generate a statistically correlated afterpulse to the original avalanche triggered by an incident photon [9, 14, 44].

To efficiently and accurately perform experiments we must also account for all non-ideal behavior of the detectors used [40, 45]. In this work I will present the operation and characterization of APDs with an emphasis on a typical ill effect of APDs known as afterpulsing.

An ideal detector emits one and only one output electronic pulse for an incoming photon but unfortunately due to the semiconductor medium or the electronic circuits of the detector, they suffer from many non ideal characteristics. Including the generation of more than one electrical signal for each incident photon [40]. An afterpulse click is also a detection event as reported by the detector.

The resultant over estimation of counts due to afterpulses is a critical problem for most applications. Especially when using an active quenched APD, which suffers from this imperfection. Unlike active quenched detectors, passive quenched detectors do not suffer from this drawback. Due to the extended dead time in passive quenched detectors – introduced due to an approximately magnitude higher dead time – trapped carriers are given time to be released. Thus these carriers will not re-trigger the avalanche when its bias voltage is returned above breakdown. In passive quenched APDs most of the afterpulse effect is suppressed and plays a negligible role.

[5] Deep levels are located at intermediate energies between the conduction band and the valence band and can act as minority carrier traps

In active quenched detectors, it is possible, to ignore all clicks a few hundred ns after any detection event. This effectively increases the dead time and avoids the bulk of afterpulses but this severely limits the maximum count rates and detection efficiency due to saturation-like effects.

However, in many applications it is of great importance to have high count rates, therefore active quenched APDs are mostly used, preferably with short (well below 100 ns for Si APDs) dead times. However due to it's shortened dead time, it can not only detect high count rates but also a significant amount of the afterpulses are additionally detected. Improvements in quenching circuits might lead to even faster APDs (with even shorter dead times) and higher afterpulsing probability. In the future, this APD drawback might gain in importance since most applications of APDs are hindered by afterpulsing. Although in many cases these ill effects can be corrected for in post-processing. However, to do so one must characterize each detector individually as evidenced by the large variation in the afterpulse probabilities between detectors of the same model number, age and manufacturer under almost identical laboratory test conditions.

## 2.6 Afterpulsing models

For many years, afterpulsing has been extensively studied from a semiconductor physics based perspective. Several conflicting studies have tried to model afterpulsing behavior and link it to fundamental semiconductor physics [4, 12–15, 17, 18], where it is important to understanding how trapped charges/energy levels decay. It is interesting to note that due to this assumption of linking the afterpulse effect to the semiconductor levels, there are so many different models about afterpulsing.

### 2.6.1 Multiple Exponential Model

Since the characteristic decay of afterpulse probability was thought to depend on the deep level of the semiconductors. Initial models considered several distinct deep levels between the conduction and valence band, where the carries can be trapped. Several experiments [13, 35] have assumed that the nature and concentration of deep levels determines the afterpulsing effect. Since the process of depopulation in solids is typically exponential [14, 16], the multiple exponential model was first proposed by Cova et al., where the afterpulsing probability ($P_{exp}$) is defined by:

$$P_{exp}(t) = \sum_k A_k e^{-\frac{t}{\tau_k}} + d, \tag{2.1}$$

where $\tau_k$ and $A_k$ is the de-trapping lifetime and amplitude factor for the $k^{\text{th}}$ deep level, and d is the offset due to noise counts. In the fitting procedure $A$ refers to the amplitude and $d$ to the offset.

### 2.6.2 Power model

The Power model was first proposed by Itzler et al. [4] to characterize the afterpulsing behaviour in an InGaAS/InP detector. The canonical approach to ascribe deep levels with exponential carrier de-trapping lifetime, which dictate the afterpulsing behavior is replaced by a single power law function. Itzler et al. [4] came to a conclusion that extracted de-trapping time constants of the multiple exponential model have no physical significance and show it can be easily interchanged with a more simple empirical model – the so called Power model (see Equation 2.3).

This power model was primarily shown to be effective for InGaAS/InP detectors [4, 46, 47]. Now, we show that it is a reasonably good model for the two different types of Si detectors (SPCM-AQ4C and $\tau$-SPAD-fast) we tested whiling failing for other two manufacturers SPCM-NIR and id100-MMF50 [16]. We provide a detailed analysis in the Section 3.4.

This empirical derived model first described in Refs. [4, 47] is based on an assumption that by integrating over the inverse de-trapping rate distribution D(R) [6] one obtain the afterpulsing probability [4]. The afterpulse probabilty can be approximated by:

$$P_{pow}(t) \approx \int_{\tau_{min}}^{\tau_{max}} dR\, D(R)\, R e^{-t\,R}, \tag{2.2}$$

whereas the afterpulse probability is directly related to the temporal change in trap occupation $N$ given by $dN/dt \approx R\, e^{-tR}$ with $t$ to be the hold-off time and $\mathrm{R} \equiv 1/\tau$ the de-trapping rate. The integration limits ($\tau_{\min} = 10\,\mathrm{ns}$ and $\tau_{\max} = 10\,\mu\mathrm{s}$) are deduced from obtained experimental data. After integration of the Equation 2.2 over the integration limits, the models output shows a power law behavior $P_{pow}(t) \approx t^{-\lambda}$. Since the model's output is consistent with their experimental results, the afterpulse probability is propose to be described by the power model ($P_{pow}(t)$) given by:

$$P_{pow}(t) = A \cdot t^{-\lambda} + d, \tag{2.3}$$

where $\lambda$ is an effective decay constant and $A$ is the the initial afterpulse probability. In the fitting procedure $A$ and $d$ are the fitting parameters of the function.

[6] It is assumed that the D(R) = C is an uniform distribution of detrapping rates D(R) with C being some constant [4].

### 2.6.3 Hyperbolic Sinc Model

In an another attempt to create a more physically meaningful, [16] derived the so-called "hyperbolic Sinc model". Thus, upon examining the power model and multiple exponential model fitting procedure, [16] hit upon the idea of having a quasi-continuous distribution of deep levels with energies between some values $\epsilon_{min}$ and $\epsilon_{max}$.

The discrete deep levels model – the multiple exponential model (see Equation 2.1) – is replaced with an assumption of constant density of populated levels per increment of energy. Here it is assumed that we have a continuum of levels, where the afterpulse probability is given by:

$$P_{sinc}(t) = \int_{\epsilon_{min}}^{\epsilon_{max}} \gamma(\epsilon) e^{-\gamma(\epsilon)t}\, dU(\epsilon) + d, \tag{2.4}$$

where $\gamma(\epsilon) = 1/\tau(\epsilon)$ is the decay rate of the corresponding deep level and $U(\epsilon)$ the combined probability of a carrier in active area producing an avalanche ($P_{aval}$) and total population of deep levels ($A_\epsilon$) with energies below or equal to $\epsilon$ just after the expiration of dead time [16]. In this model, $U(\epsilon)$ is equivalent to the $A_k$ – the amplitude factor for the $k^{th}$ deep level of the multiple exponential model.

Furthermore, the decay rate $\gamma(\epsilon)$ of deep levels used in this equation was proposed by [17], where it shown that it might follow the Arrhenius law [7]:

$$\gamma(\epsilon) = B\, e^{-(\epsilon-\epsilon_0)/kT}, \tag{2.5}$$

where $B, \epsilon_0$ are constants akin to the semiconductors band structure, $T$ is the temperature and $k$ is the Boltzmann constant. Next, the $\mathrm{d}U(\epsilon)$ can be written as $\mathrm{d}U(\epsilon) = A\mathrm{d}\epsilon/(kT)$ and substituited into Equation 2.4, and then integrating over the integration limits ($\epsilon_{min}$ to $\epsilon_{max}$), this brings us to:

$$P_{sinc}(t) = 2 \cdot A \cdot \frac{\sinh(\Delta \cdot t)}{t} \cdot e^{-\gamma \cdot t} + d, \tag{2.6}$$

where $\Delta$ and $\gamma$ are both functions of the minimum and maximum energies of the deep levels in which charges may be trapped.

[7] Arrhenius' equation is originally used to determine the rate of chemical reactions for a certain energy of activation. It is define as following $k = A\, e^{E_a/kT}$, where $E_a$ is the activation energy for the reaction, which in our case would refer to the activation energy of the trap, $T$ is the temperature, $k$ is the Boltzmann constant and $A$ (pre-exponential factor)

# Chapter 3

# Can afterpulsing be attributed to the semiconductor's band structure?

In this chapter I provide a detailed analysis of the afterpulsing effect by comparing different canonical models and detectors brands (Excelitas, PerkinElmer and Laser Components) among each other. The proposed models (as described in Section 2.6) attempts to explain the afterpulses behaviour (solely) based on the presence and distribution of discrete/continuous/quasi-continuous deep levels in the detector's semiconductor. Using the experimental setup as shown Section 3.2, we were able to show in Section 3.4 that none of the current theoretical models are universal nor can we draw any qualitative conclusion about the inner structure of the APD such as the semiconductor's band structure.

Moreover, using the cross-correlation function (as discussed in Section 3.1) to investigate the afterpulse effects, I was also able to show higher order of afterpulses as discussed in Section 3.5 in one make of detectors we tested. Although these higher order afterpulses has been mentioned in Refs. [4], it has never been reported nor accounted for in any of the standard models of afterpulse behaviour.

## 3.1 Introduction

Initial studies [14, 48] used the Time-Correlated Carrier Counting (TCCC) technique for characterisation of afterpulsing effect. Originally this technique was used in semiconductor research especially fluorescence spectroscopy. It was developed for direct determination of the effective minority-carrier lifetime. Since it has been suggested that afterpulsing can be linked to charges trapped in the deep levels of the semiconductor's

band structure [14]. Therefore, afterpulsing effects can be evaluated by using the time-correlated carrier counting technique as described in Refs. [14, 48].

Cova et al. [14, 48] have demonstrated afterpulsing behavior by analyzing the temporal sequence of output signals of the APDs. These electric pulses measured are attributed to released carriers. The signals were then split into two coaxial cables by a balanced impedance (50Ω). One signal is delayed with respect to the other and one is used as the Start signal and the other as the Stop signal. The delay between Start and Stop is converted into a temporal correlation histogram [14, 48].

Since then modern techniques have been developed [45, 49] e.g. investigation of the statistical distribution of the times between consecutive detections to obtain afterpulses. Most recent works [15–17, 45] have demonstrated afterpulsing effect by this method. Hummer et al. [15] measures the output pulses of the APDs using a time-to-digital converter. They make use of an time-tagging-module (TTM) to record all start and stop signals on a single channel and consequently the time delay between them is used to compute an auto-correlation function.

In this chapter I will present my contribution in the study of afterpulse effect by performing the first comparative study of afterpulsing behaviour in various makes/brands of detectors and probing for the causes of the contradictions between previously proposed standard models. Unlike previous measurements, I will eschew the common practice of studying the timing auto-correlation of the APD signals in favor of the more comprehensive timing cross-correlation between the emission of a photon and all the subsequent APD signals. This is allows me to analyze the behaviour during the dead time and the presence of higher order afterpulses.

## 3.2 Setup

The general scheme of the setup used for the experiments is shown in Figure 3.1. The function-generator is used to trigger the 798 nm laser. The laser generates optical pulses with a 1 ns pulse width and various repetition rates between 0.25 to 1 MHz.

The custom built laser from our collaborator (M. Stipčević[1]) had to fulfill two crucial properties in order to do a proper analysis of the afterpulsing behaviour. Besides, producing a narrow pulse width of $\approx$ 1 ns there is a technical challenge to have the laser diode completely switched off between two consecutive laser pulses. It is a common practice to turn the laser diode off by operating just below the threshold level. However, using this method the laser diode is not completely off and still emits a significant amount of photons. Since we operate at a single photon level, these additional photons

[1]Ruder Boskovic Institute, Center of Excellence for Advanced Materials and Sensors and Division of Experimental Physics, Zagreb 10000, Croatia

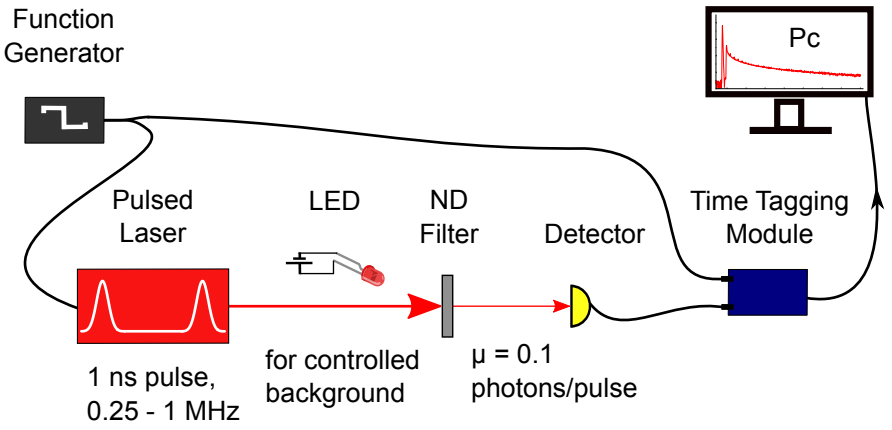


**Figure 3.1:** The experimental setup showing the 798 nm laser that is used to generate pulses with a 1 ns pulse width and 1 MHz repetition rate. The Neutral Density (ND) filters are used to attenuate the laser pulse and control the number of detected photon per laser pulse in the APDs.

emitted can not be neglected. Therefore, our laser is made so as to prevent it from emitting photons when it is operated below the threshold level.

To affirm that no significant detection events originate from the laser when operated below the threshold level, we characterized our laser. By analyzing the laser pulse profile, we could determine that no significant additional peaks occur in the laser pulse profile, which could skew our results and be responsible for the afterpulses in the $g^{(2)}$ histograms (see Figure 3.2).

We used a battery powered Si-Biased detector from Thorlabs (DET10A/M) and recorded the laser pulse profile with an oscilloscope (LeCroy WavePro 760Zi). Before we can perform our laser pulse profile measurement, we measured the dark voltage of the Si-Biased detector. This allows us to estimate the contribution of electronic noise, background noise etc that could distort our results of the laser pulse profile. To do so, we covered the Si-Biased detector with a black cloth to block as much background counts as possible and connected it to the oscilloscope without having the laser diode physically in the experimental setup. The measured value for the dark voltage of our detector was 50 mV. Then, in the next step, the laser pulse profile was measured under the same conditions (see Figure 3.2). As shown in the Figure 3.2, we observe some small peaks in the tail region of the laser pulse peak. We investigated these small peaks, to rule out these peaks as a source of the afterpulses in our temporal cross-correlation histogram ($g^{(2)}$).

By converting the output power of our photo diode, we were able to estimate the number of photon counts corresponding to these small peaks/pulses. After applying the dark voltage correction to our data and we can convert the output power into number photons and obtain $4{\cdot}10^8$ photons/s [2].

[2]The number of photons per second is given by Photons/s $= \frac{P\lambda}{hc}$, where $P$ is the power in watts, $h$ is Planck's constant, $\lambda$ the wavelength and $c$ is the speed of light.

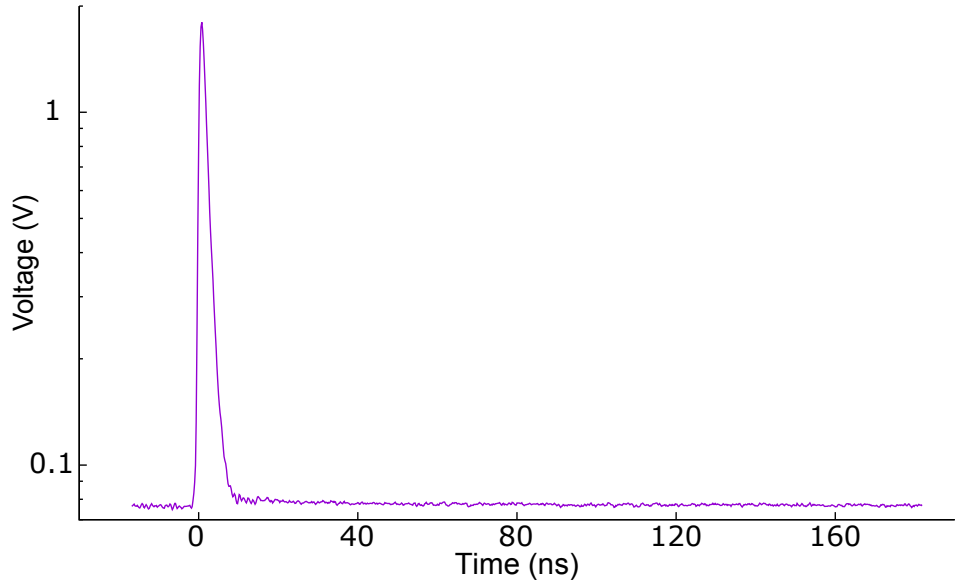


**Figure 3.2:** Laser pulse profile measurement using fast photodiode with a 2 GHz bandwidth while recording the data with an oscilloscope (LeCroy WavePro 760Zi). The graph shows one main peak with no significant pulses afterwards that could result in a subsequent event skew our temporal cross-correlation histogram ($g^{(2)}$).

Further, we used a ND 10 filter (with a transmission of $10^{-10}$) in our experimental setup to attenuate the laser pulse. Therefore, only an average of 0.04 photons/s passes through the filters. Including the detection efficiency of the APD into our assumption, we get $\approx$ 0.02 photon counts/s. The contribution of these small peaks are two magnitude lower than the dark counts of our APDs. Depending on the make/manufacture of detector, we have $\approx 100$ - 200 dark counts/s.

Moreover, as depicted in Figure 3.2 these small pulses are $\approx$ 5 to 10 ns apart from the actual pulse, therefore do not match the afterpulse timing. The earliest possible afterpulse we detect with our detectors SPCM-NIR from Excelitas are $\geq$ 22 ns after the signal pulse (see Figure 3.7). On the whole, the emissions from the laser after attenuation by ND filters can contribute to a maximum relative error of 0.3 % in our measurement of the afterpulse probability. Consequently we assume that the effects due to laser imperfections on our calibration of the detectors is negligible.

As mentioned earlier in this section, we attenuate the emitted light using Neutral Density (ND) filters until we have $\ll 1$ detected photon per laser pulse on average (we get this value assuming the detection efficiency of the used APD). Further, we use two channels of the time tagging module (TTM8000) to record the trigger from the laser pulse in Channel 1 and photon detection event in Channel 2. We consider the first event arriving at the TTM (from the single photon detector), after a given laser pulse to be the "detection pulse" which stems from the real photon impinging on the active area of the detector. Any further detection events after the initial one is a result of either afterpulsing or

noise. We do not distinguish between the different origins of the pulse[3]. It can be due to some secondary avalanches in the semiconductor diode caused by thermal effects, the quenching circuit or background noise. After recording the data, we compute the temporal cross-correlation histogram ($g^{(2)}$) between the trigger signal from the function generator and APD signal with a bin width of 1 ns using a software I wrote to process the acquired data (see Section 3.3).

## 3.3 Data collection and data processing

We wrote a software to processes the data from the time-tagging module and to compute the cross-correlation function to investigate the afterpulse behaviour.

In order to understand the data processing steps let us first look at the data collection. Using the software Time Tagging Control Center and TTM Viewer - Data Source [4], we were able to collect the data. We expect the afterpulsing probabilities to be in the magnitude of 0.1 % to 10 %, therefore we collect a significant amount of data (beyond $10^8$ detection events) to even see marginal changes of some ppm in the afterpulse probability. This is also the reason for we decided to collect the data in binary format.

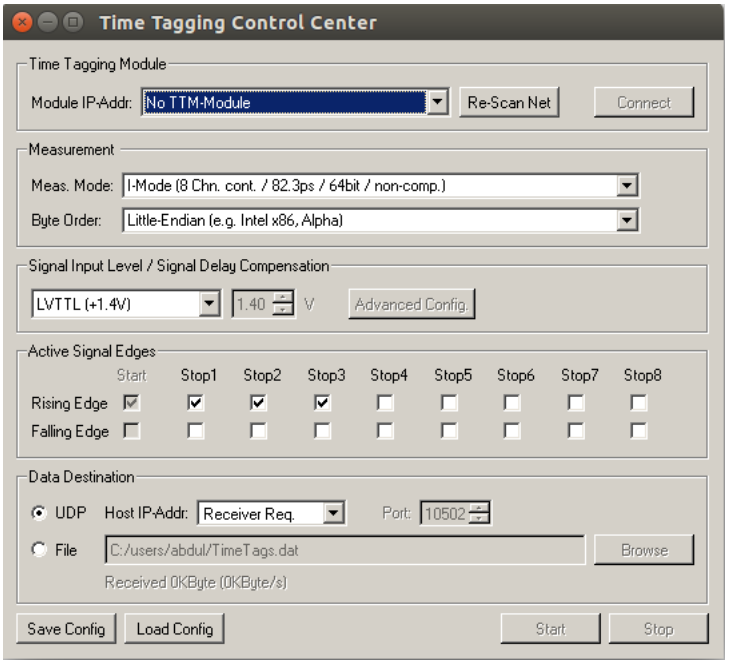


**Figure 3.3:** The Time Tagging Control Center is used to connect the TTM module and select the measurement mode for the data collection.

[3]From an end user perspective, it is impossible to discriminate between pulses of different origins. We too do not distinguish pulses based on their physical origin because to do so would defeat the purpose of calibrating the detector for each usage scenario. Further, we note that due to the impossibility of an end user differentiate pulses based on their physical origin, all previous studies, including those advocating various models based on semiconductor physics, also do not distinguish between pulses based on their cause.

[4]Both of the software are provided by Roithner Lasertechnik

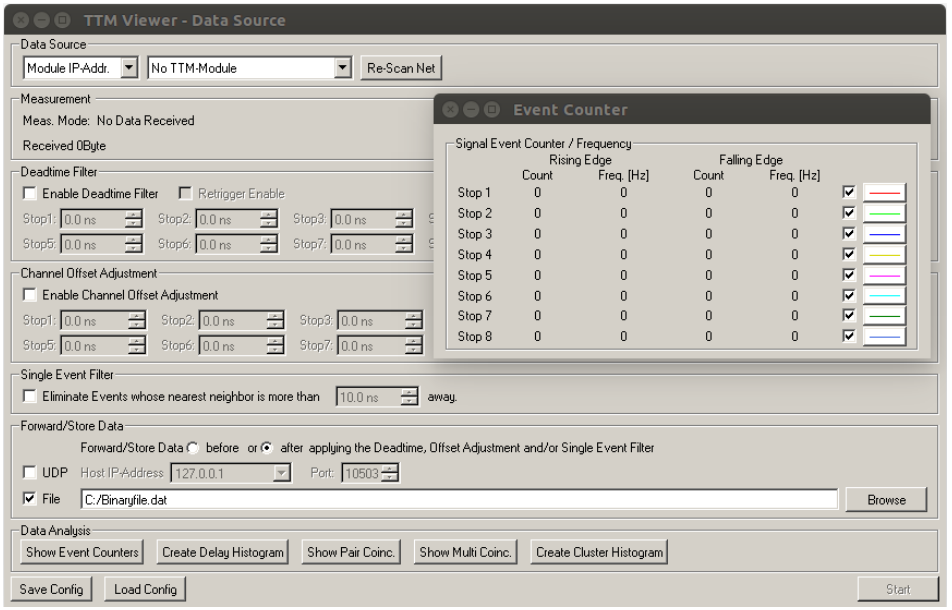


**Figure 3.4:** With the TTM Viewer we collect the data and use it as a preview tool to monitor the detection events while performing the experiment

We used the TTM Converter (TTMCnvt) to change these binary files into hexadecimal data type. Now, we have hex files consisting of 3 columns with the following information channel/slope/timetag [5](see Figure 3.6).

The final step was to write a python script [6] in order to determine the time delay between two signals. In our case, we compute the cross-correlation between the two channels of the time tagging module we used (Channel1 recording the trigger from the laser pulse and Channel 2 the photon detection event).

### 3.3.1 Cross-Correlation

Traditionally, the auto-correlation function has been used to characterize the afterpulsing behaviour, however in most recent works it is still the only method used for afterpulsing investigation. Although the auto-correlation function is a useful method due to a variety of reasons, nonetheless the cross-correlation gives all the information as auto-correlation and even more e.g. the timing correlation between the detector and photon source.

Firstly, since the auto-correlation is a correlation of a signal with a delayed copy of itself, it requires much less data and hence has a faster computation. Secondly, in comparison to cross-correlation function, where an irregularly pulsed laser introduces a timing jitter, we do not the same issue in an auto-correlation histogram. Furthermore, knowing that an

[5] A timestamp given by the time-tagging unit denoting the arrival of an signal.

[6] We chose Python as our programming language because it easy to handle, the code it easy to read and object oriented.

auto-correlation being the inverse Fourier transform of the power spectrum, computing an auto-correlation of our laser pulse we can check for noise in the laser histogram.

On the contrary the resultant histogram using an auto-correlation has no information for the period of time before the detector dead time [16]. This explains why all previous works on afterpulsing behaviours, regardless of model only characterized the timing structure of the tail.

Yet, with the use of cross-correlation functions, it allows us an investigation of the behaviour during the dead time and also report on the presence of high order afterpulses. This has not been observed nor accounted for in any of the standard models of afterpulse behavior. New technology, scarifying computing time due to cross-correlation, storage of high amount of data, and a well defined pulsed laser, put together, makes it possible to perform this new method of investigation of the afterpulsing behaviour.

With the advent of modern technology like time-tagging units to record all signals on a single channel, improvement in computational power simplifying the computational effort needed to compute the cross-correlation and costs reduction of time tagging unit and data storage units, it is reasonable to perform the cross-correlation with no excuse.

Measuring the auto-correlation requires one to store less data than cross-correlation and simplifies the computational effort needed. For this reason auto-correlation was the most commonly used method to analyze afterpulsing. However, auto correlation ignores the timing correlation between the detector and photon source see Appendix A for more details.

The mathematical definition of the correlation of a time function $\mathrm{Ch}_1(t)$ correlated with another time function $\mathrm{Ch}_2(t)$ is defined by the Equation 3.1. Here, one of the functions is shifted with respect to the other [11] and can be written as:

$$\mathrm{G}_{12}(\tau) = \mathrm{Ch}_1(t) \oplus \mathrm{Ch}_2(t) = \sum_{t=-\infty}^{\infty} \mathrm{Ch}_1(t)\,\mathrm{Ch}_2(t-\tau) = \sum_{t=-\infty}^{\infty} \mathrm{Ch}_1(t+\tau)\,\mathrm{Ch}_2(t) \tag{3.1}$$

In case of an auto-correlation, which shows the correlation between the function $\mathrm{Ch}_1(t)$ with itself, we obtain:

$$\mathrm{G}_{11}(\tau) = \mathrm{Ch}_1(t) \oplus \mathrm{Ch}_1(t) = \sum_{t=-\infty}^{\infty} \mathrm{Ch}_1(t+\tau)\,\mathrm{Ch}_1(t) \tag{3.2}$$

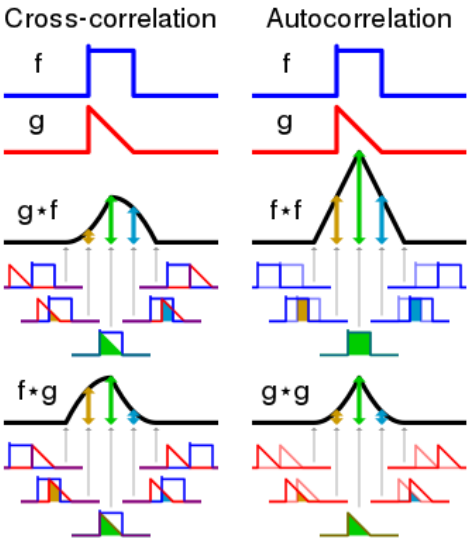


**Figure 3.5:** Here we can see the visual comparison of cross-correlation and auto correlation. Further, we can observe the change in cross-correlation depending on if we perform a $\mathbf{g} * \mathbf{f}$ or $\mathbf{f} * \mathbf{g}$ [11].

In case of a stationary process [7], the cross-correlation function (see Equation 3.1) can be simplified and is only dependent on the time difference $\Delta t = (t_2 - t_1)$ between the two functions. By doing preliminary tests, we verified to have a stationary process, which means the detection events and the trigger signal of the laser pulse show no time dependence. Beyond that, we collect millions of detection events. Consequently, we assume that if there are time dependence effects due to laser imperfections or detector's temperature or etc., they are negligible.

In order to implement the cross-correlation function in our program, we converted the hexadecimal timetags into readable integers and ignore the redundant second column containing the information about the slope. Further, we extract the information about the channel and its related timetag to create two separate data sets. Now, we have subsets (subsetA & subsetB) accommodating all timetag entries ($t_i^{(Ch1)}$ & $t_j^{(Ch2)}$) for each channel. By calculating the time delay $\Delta t = (t_i^{(Ch1)} - t_j^{(Ch2)})$ between these timetags, we obtain the delay histogram between the trigger signal of the laser and detection event in our APD (see Figure 3.7) (See the source code in Appendix B for more details).

In the next step, we apply normalization and accidentals corrections (we discuss the corrections in Section A) to the histogram. We correct our data for these accidentals [8] before applying the normalization.

[7] A stationary process is a stochastic process whose joint probability distribution does not change when shifted in time. Consequently, parameters such as mean and variance, if they are present, also do not change over time.

[8] In typical quantum optics experiments, there is a probability that a coincidence is detected between two different detectors erroneously, we call these coincidences "accidentals". In our case it refers to a detection event in absence of a real photon from the source although there has been a trigger pulse from the function generator

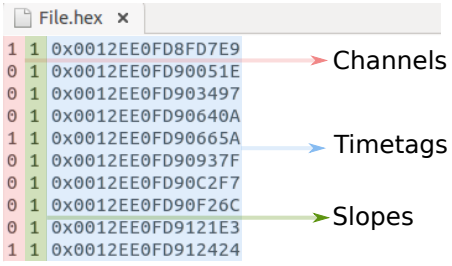


**Figure 3.6:** An example of a hexadecimal data type file containing the channel/slope/timetag.

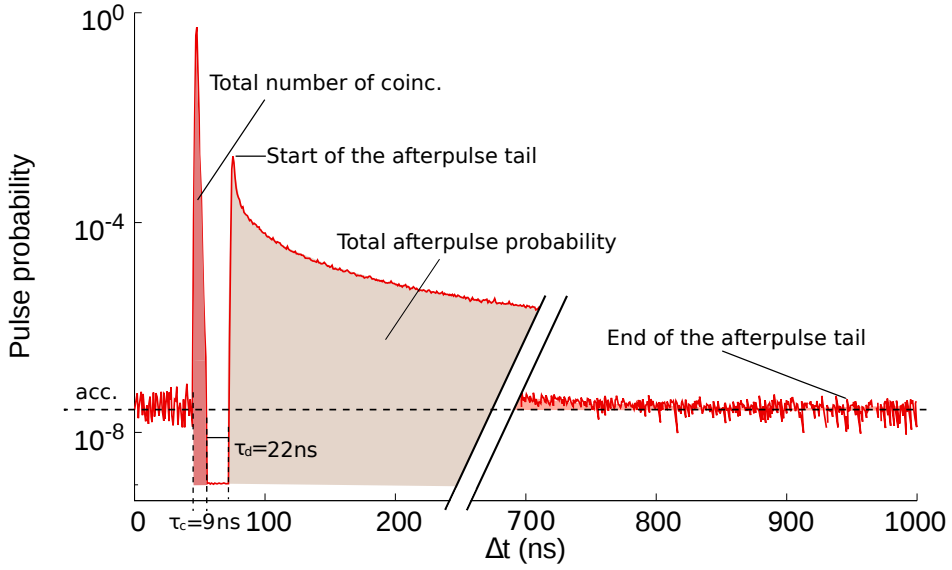


**Figure 3.7:** Accidental level and normalization factor

We estimate the rate of accidental coincidences in our histograms by using a region far away from any peak. As shown in Figure 3.7 we choose the first 50 ns in our $g^{(2)}$ histogram to compute an average accidentals rate. In this region before the main peak, we are convinced to have no potential coincidence counts from the afterpulse tail that could skew our results.

To obtain the total number of coincidences detected (normalization factor), we integrate over the entire signal peak in a region given by $\tau_c$ and attain the pulse probability in each individual bin and subsequently the total pulse probability. We ensured that this integration includes almost all coincidences, while avoiding adding any redundant accidentals.

Next, we fit each of the standard models (see Equations 2.1, 2.3 and Equation 2.6) to the tail of the afterpulse for each different APD. In all previous works on afterpulsing behaviours, regardless of model only the timing structure of the tail is characterized. The afterpulses were linked to charges trapped in the deep levels of the semiconductor's band structure as mentioned earlier in Appendix 2.5. Since the process of depopulation in solids is typically exponential, it is sufficient to study only the tail of the afterpulse peak in order to extract useful information about the characteristic decay of afterpulses.

The rising edge of the afterpulse peak is not included into the standard models, because it does not provide any qualitative information about the underlying mechanism within the semiconductors. Further, due the jitter in the electronics, it is a huge challenge to detect this very fast rising edge precisely. Even so, it varies from detector to detector and the time tagging unit used. Although the study of the rising edge on afterpulse pulses of APD's in general is an interesting avenue for further exploration, it would go beyond the scope of this experiment.

Furthermore, in order to compare these standard models with each other, we isolate the tail of the afterpulse from the rest of the histogram and only fit this particular region. For our fitting region we choose the peak (referring to 0 in our $g^{(2)}$histogram see Figure 3.10) as a starting point and a value of 900 ns as end point of the tail such that we include a significant amount of the afterpulse tail while avoiding any potential effects due to the earliest possible subsequent pulse 1 $\mu$s later. In addition, we verify that at the chosen value the tail has faded into accidentals. The duration of the afterpulse tail does not varies significantly from manufacturer to manufacturer we tested.

To determine the best fit for all 3 models, we used the Least Squares Fitting method. Upon, examining various fitting algorithms (Levenberg-Marquardt, Nelder-Mead, Powell, Truncated Newton, Sequential Linear Squares Programming, etc.), we did not discover any improvements nor preference of an algorithm for a model.

## 3.4 Comparison of afterpulsing models

Figure 3.8 shows the resultant $g^{(2)}$ histogram for each different APD. We can clearly identify the signal pulse and the afterpulse being well separated by the so called "dead-time". On can also see the region of interest - the afterpulse tail. The tail of the afterpulse of all APDs are shown in Figure 3.8 after normalization and accidentals correction have been applied (as discussed in Section 3.2).

We observed a wide variation between different detectors we tested from each of three manufacturers. We saw a drastic change in the total afterpulse probability between otherwise identical detectors. In some cases we even measured significant changes in the total afterpulse probability for nearly identical detectors. As is the case with $\tau$-SPAD-fast detectors (with serial number 01019917 and 1019920), having once a total afterpulse probability of 5.1$\pm$ 0.003 % and 8.5$\pm$ 0.002 %.

To ensure that our results are not skewed by any fluctuations in temperature, laser power, electronic noise, optical reflections or stray light we tested the detectors of each type multiple times on different days and with different settings. Furthermore, using a beam splitter we were able to run the experiment simultaneously and have same conditions for multiple detectors. However, each identical detectors of the same manufacturer,

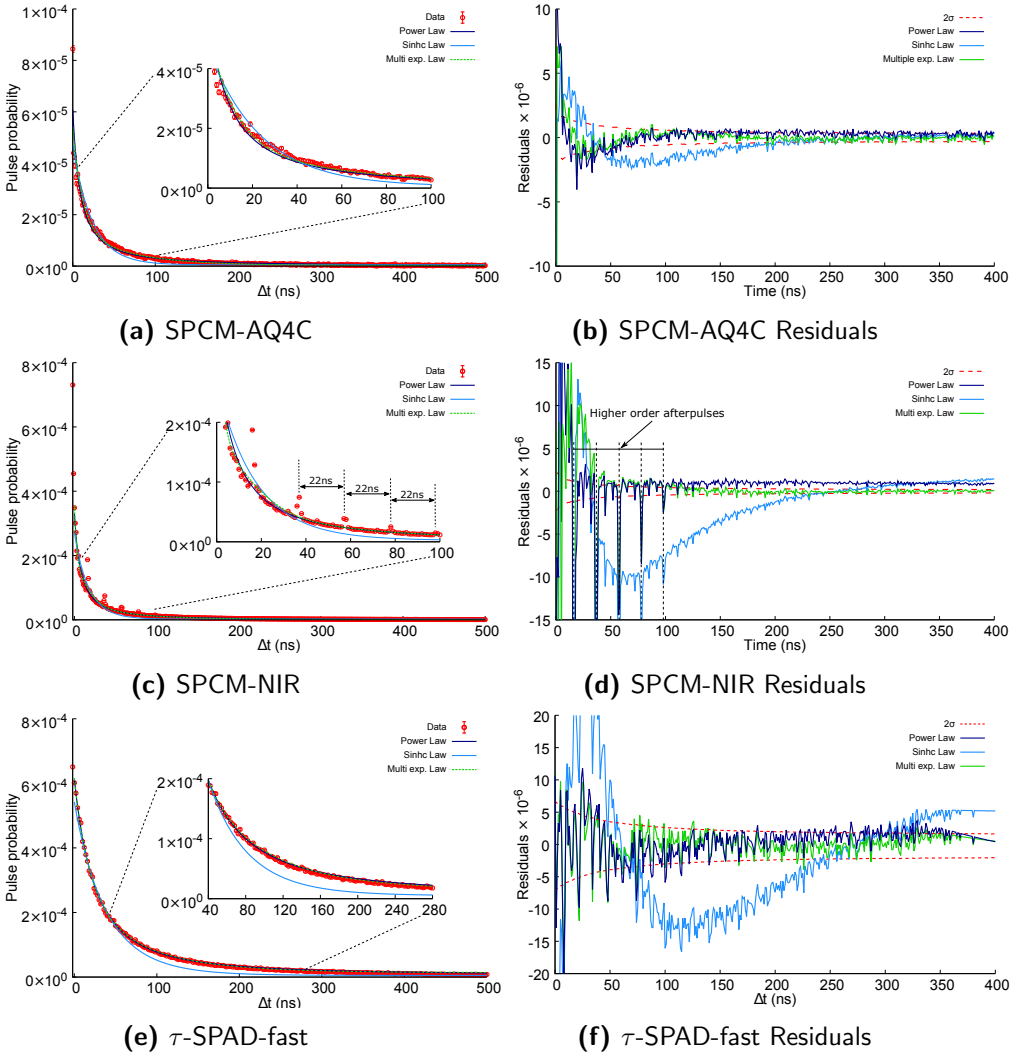


**(a)** SPCM-AQ4C **(b)** SPCM-AQ4C Residuals

**(c)** SPCM-NIR **(d)** SPCM-NIR Residuals

**(e)** $\tau$-SPAD-fast **(f)** $\tau$-SPAD-fast Residuals

**Figure 3.8:** Afterpulse peak's tail fitted with Power model, Hyperbolic-sinc model and multiple exponential model for SPCM-AQ4C (PerkinElmer), SPCM-NIR (Excelitas) and $\tau$-SPAD-fast (Laser Components) - Comparison of residuals for all detectors and models (Power model (blue), Hyperbolic sinc model (cyan) and Multiple exponential model (green)) and the red dashed lines are $\pm$ 2 standard deviation limits for statistical fluctuations. We analysed $> 0.14\times10^6, 2.7\times10^6$ and $3\times10^6$ *afterpulse* events for each SPCM-AQ4C, SPCM-NIR, and $\tau$-SPAD-fast detector we analysed respectively.

had nearly the same fitting parameters for the same model. The only significant difference between two $\tau$-SPAD-fast detectors was the amplitude factor $A$, which caused the difference in the total afterpulse probabilities.

On the whole, unlike the hyperbolic Sinc model, the Power model approximates the experimental data more accurately independent of the APD used (AQ4C, SPCM-NIR, $\tau$-SPAD-fast). One can clearly see in Figure 3.8 that the Power model is fitting the entire range of the tail better than the Hyperbolic sinc model. In case of the hyperbolic sinc model, we consistently obtain unsuitable fits to our experimental data especially in SPCM-NIR and $\tau$-SPAD-fast.

As depicted in Figure 3.8 and having the entire afterpulse shape in mind, one can

determine that the Hyperbolic sinc model gets even worse the shallower the afterpulse peak e.g. $\tau$-SPAD-fast. In addition, initial guesses for the hyperbolic sinc model are very crucial to fit the experimental data, whereas the power law has no trouble fitting the afterpulse tail nearly independent of the chosen values.

The goodness of the fits can be quantitatively compared using the residuals seen in Figure 3.8 with the $\pm$ 2 standard deviation range (shown in red). From Figure 3.8 we can determine that the Power model is well within 2 standard deviation for SPCM-AQ4C and $\tau$-SPAD-fast, whereas the hyperbolic sinc model is nowhere near to an optimal approximation of the experimental data.

The Power model was primarily shown to be effective for InGaAS/InP detectors [4, 46, 47] and we now show that the Power model as a simple analytic model function leads to reasonably good results (as seen in Figure 3.8) for the different types of Si detectors we tested.

However, it's extracted fitting parameters gives a rather loose description of the physical origin of afterpulses. A truly good model should be able to predict the behavior of the entire tail region (without ignoring certain regions of the afterpulse peak). The Power model like the other two models (hyperbolic sinc model and multiple exponential model) only provide a suitable fit if the beginning of the afterpulse tail is ignored.

The multiple exponential model provides a good fit when at least 5 exponential functions are used for fitting the aftepulse tail and than it is slightly better than the Power model especially for the SPCM-AQ4C detector. It is nearly commensurate with the Power model for the $\tau$-SPAD.

For the SPCM-NIR, the exponential model gives a good fit only when we ignore the higher order afterpulse peaks (which are discussed in Section 3.5). We observed that it was possible to get different fits of almost the same quality with different characteristic times $\tau_k$ (also called the de-trapping times) depending on the number of exponentials used. Thus, upon examining the fitting procedure we concur with [4] who state that "It is evident from this whole fitting procedure that the extracted values for the de-trapping times depend entirely on number of exponentials in the model function and the range of hold-off times used in the data set." It is hard to believe that these obtained values from the exponentials fits have any physical meaning.

Unlike previous studies Horoshko et al.[12] proposes a new model, the so called Hyperbolic-sinc model (as discussed in Section 2.6.3) fitting his experimental data of one particular brand of detector (id100-MMF50 APD module from idQuantique). Horoshko et al. results (see Figure 3.9) contradicts to previous studies and completes the picture that there is no universal theoretical models to explain the afterpulse behaviour.

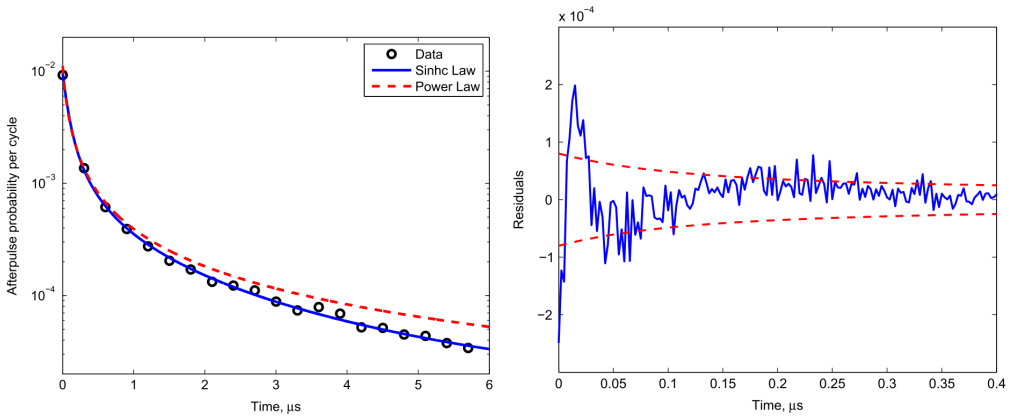


**(a)** idQuantique - id100-MMF50

**(b)** Residuals for the hyperbolic sinc model

**Figure 3.9:** A comparison between Power model and Hyperbolic-sinc model studied in [12] shows that in this particular make of detector (id100-MMF50 APD module from idQuantique), they have a better result for a Hyperbolic-sinc model. **(a):** Afterpulse peak's tail fitted with Power model and Hyperbolic-sinc model. **(b):** Residuals of the hyperbolic sinc model (blue) and $\pm 2$ standard deviation limts for statistical fluctuations for the first 400 ns of the fit.

| | Detetor used | Best model according to study |
|---|---|---|
| A. C. Giudice, Italy [13] | PerkinElmer SPCM SliK™ | Multiple exponential model |
| D. B. Horoshko, Belarus [16] | idQuantique id100-MMF50 | Hyperbolic sinc model |
| G. Hummer, Vienna [15] | Self-designed | Multiple exponential model |
| M. A. Itzler, USA [4] | InP/InGaAs SPADs | Power model |
| **This thesis** | PerkinElmer SPCM-AQ4C, Excelitas SPCM-NIR and Laser Components $\tau$-SPAD-fast | Multiple exponential model |

**Table 3.1:** Table comparing various outcomes of studies on afterpulses. We can see that none of the canonical models are universal. Previous efforts to find a universal and fundamental model of afterpulsing are perhaps futile.

## 3.5 Higher order afterpulses

Considering that any detection event may cause an afterpulse, it already indicates that an afterpulse may induce secondary and further afterpulses which we call "higher order afterpulses". The presence of such higher order afterpulsing was first speculated in [4] but, to the best of our knowledge, never reported. It has also not been observed and it has not been accounted for in any of the standard models of afterpulse behavior. Usually afterpulsing is a small effect and the afterpulsing probability distribution function is smeared such that the higher order afterpulses are improbable. However, since every afterpulse can re-trigger secondary avalanches therefore higher order afterpulses probabilities depend on the probability of previous afterpulses. This means, that with the use

of novel detectors e.g. $\tau$-SPAD-fast (with an afterpulsing probability of up to $\approx 10\,\%$), these effects can not be neglected anymore.

In the presence of strong enough twilighting[9], photon detections and afterpulses accumulate in a narrow peak that appear just after the dead time. We note this behavior in SPCM-NIR as can be seen in Figure 3.10. The higher order afterpulses are clearly visible as a series of peaks after the main peak with a period exactly equal to the dead time of the detector.

Small peaks in the afterpulse tail of the SPCM-AQ4C detector are not due to higher order afterpulses. Perhaps, it is random data fluctuations. Firstly, it seems that the time delay between these small peaks are irregularly. It does not appear after the dead time of the detector like in case of our SPCM-NIR detectors. Secondly, testing 3 individual detectors of the same module, we were not able to reproduce any of the results.

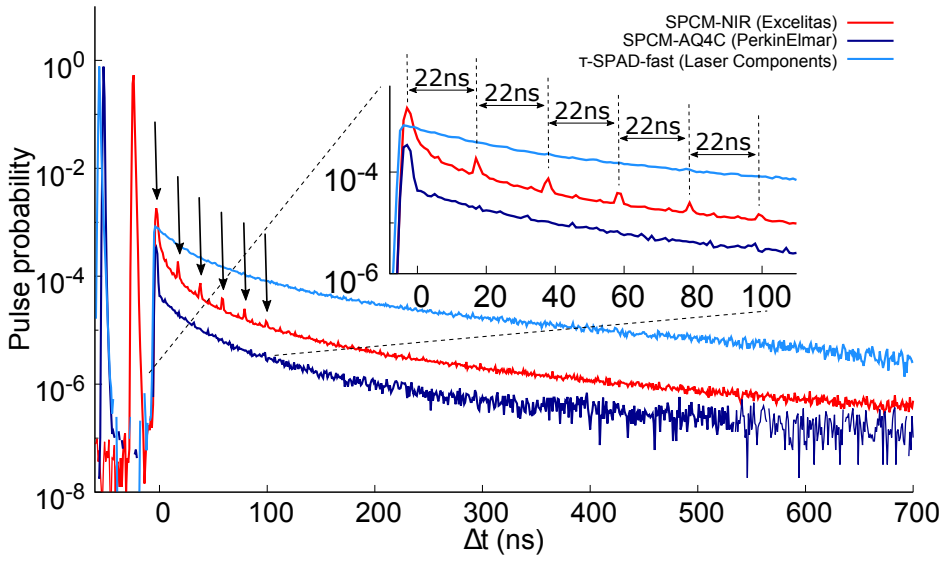


**Figure 3.10:** $g^{(2)}$ Histograms for various detectors exhibit distinct afterpulse behavior (each afterpulse peak is marked by an arrow). For example, the $\tau$-SPAD-fast displays an unusually gradual decay while the SPCM-NIR is the only detector make to exhibit higher order afterpulses. The inset shows the higher order afterpulses occurring at intervals equal to the dead time.

For the SPCM-NIR, the signal pulse and the first order of afterpulse are 22 ns apart, which exactly corresponds to the duration of the dead time of this particular detector module. The measured time intervals between all following higher orders of afterpulses (as seen in the inset of the Figure 3.10) have the same time delay of 22 ns. We have obtained a similar plot for three detectors with the same model number: in each case, peaks appear separated by the dead time of the particular detector. We observe these higher order afterpulses one due to shortened dead time of our detector and using a cross-correlation function for the computation. A prolonged dead time in the APDs

[9] Twilighting is referred to an effect when a photon is absorbed by the APD during the last moments of it's dead time, where the detector is partially sensitive to incident photons. These incident photons can re-trigger the avalanche and cause a substantially delayed pulses – the so called "Twilight" pulses [50–52]

might suppress the higher order afterpulses, but unlike previous studies [4, 13, 14, 14–18, 35, 48], we were able to discover these by investigating detectors (Excelitas SPCM-NIR) with a dead time of 22 ns. Further, these studies omitted to spot higher order afterpulses because they only looked at the time difference between the signal peak and the first order of afterpulse. The time delay between a later timed (a multiple integer of the first afterpulse) detection and the true signal was not computed.

Further, we note that it is possible to explain the area of the $n^{\text{th}}$ higher order peak based on the probability of the first afterpulse ($P(AP)$) as $P(AP)^{(n+1)}+$ the probability of an afterpulse in the bin just before the $n^{\text{th}}$ higher order peak $\times$ the number of bins in the peak. This geometric progression agrees to within 4 to 6 % for the $2^{nd}$ to $5^{th}$ order afterpulses.

We verified that the higher order afterpulses seen are not the result of stray light, the shape of the laser pulse, electronic noise, impedance mismatch or optical reflections. In addition to the room lights off, we used a black box or a black cloth to cover our setup and avoid stray light reaching the active area of the detector. We were able to get ride of spurious clicks originating form stray light and alone those due to electrical and thermal noise are detected. We achieved dark counts to less than $\approx 50$/s in case of SPCM-NIR and $\approx 150$/s for SPCM-AQ4C and $\tau$-SPAD-fast.

Optical reflection can be sorted out by having the speed of light and the dimensions of our setup in mind. Our experiment was compact with optical elements being at maximum 1 m apart, so that any optical reflection would correspond to a time delay of $\leq$3 ns in our cross-correlation histogram. However, from Figure 3.10 we can note that these higher order afterpulses (22 ns apart) can not arise from any optical reflections in the cable.

To demonstrate that these higher afterpulses are not due to any impedance mismatch or frequency variation, we vary the path length between the function generator and laser input as well as the detector output and time tagging unit, while ensuring to have the same conditions (intensity, frequency, dark counts,..) for all measurements. The essential idea behind this method is that due to an impedance mismatch the signal going through the cable can be reflected, detected more than one time and skew the results.

Consequently, if these higher order afterpulses were due to any impedance mismatch or frequency variation, we would observe a change in the timing structure of the higher order afterpulses. That means when extending the length of the cable thus the distance for the signal to be reflected, these equidistant peaks appearing in the $g^{(2)}$ histogram would change their shape and be further apart. As seen in our $g^{(2)}$ histogram (see Figure 3.11) it is not the case.

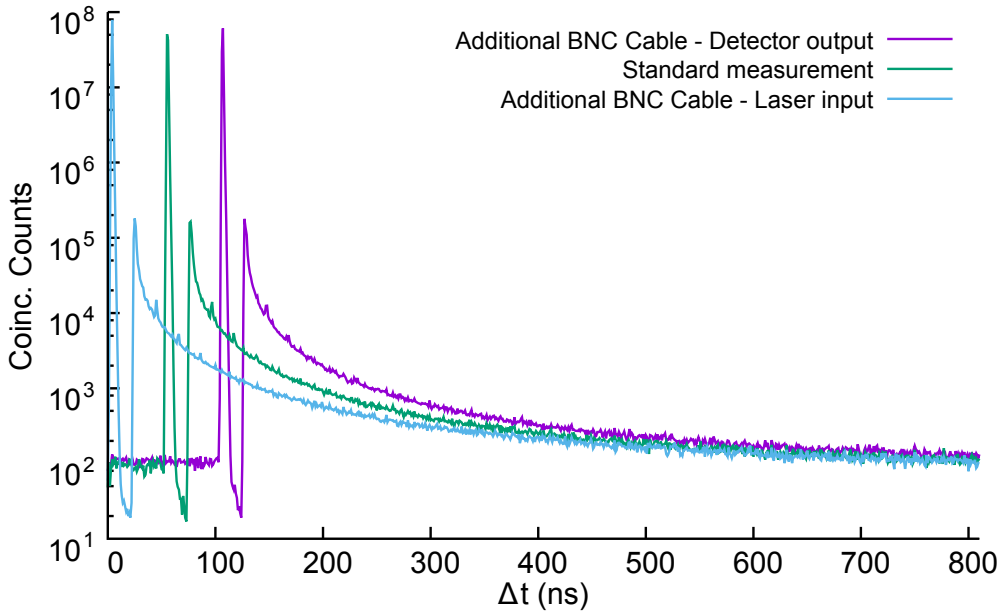


**Figure 3.11:** Change in length of the cable between the function generator and laser input (cyan) as well as the detector output and time tagging unit (violet) to check if the higher order afterpules are due to an impedance mismatch.

As shown in Figure 3.11, we only observe a shift in time ($\approx$51 ns corresponding to the time delay introduced by an additional 10 m coaxial cable) in our $g^{(2)}$ histograms, however we can still detect higher order afterpulses with same time delay of 22 ns. Therefore, we can rule out impedance mismatch or frequency variation being the origin of higher order afterpulses.

We also processed the data with different bin widths and laser pulse frequencies to ensure that the observed higher order afterpulse peaks are not due to digitization noise.

## 3.6 Conclusion

In conclusion, we can say that significant different models are required to appropriately describe the distribution of electrical signals generated by different brands/makes of detectors. This explains the conflicting nature of several previous studies; for example [4, 46, 47] show strong evidence for the Power model while [13, 14] show equally compelling evidence for the multiple exponential model and [12] provides evidence for the hyperbolic sinc model. Further, [12] showed that the hyperbolic sinc model was better than the Power model using id100-MMF50 APD module from idQuantique (see Figure 3.9), which we were unable to duplicate those results with any of our detectors.

By comparing previously reported results to our own, we realize that there is a large variation between the different manufactures and makes of detectors commonly used. The suppression of afterpulses by different quenching methods [53] leads us to believe

that the afterpulsing behavior is more dependent on the electronic quenching circuit used rather than the presence and distribution of discrete/continuous/quasi-continuous deep levels. This clearly proves that none of the current theoretical models are universal which makes it hard to draw conclusions about the underlying mechanism based on fundamental semiconductor physics.

Our results presented in this chapter shows that to efficiently and accurately perform experiments and correct for these ill effects of APDs, we must calibrate every detector individually. One can not relay on models that only seems to work for one specific brand of detector. Moreover, there is even a significant disparities between individual detectors of the same model number, age and manufacturer we tested under almost identical laboratory test conditions. This substantial change in the afterpulse tail of these detectors results in following a complete different model (Power model or Hyperbolic sinh model).

Beyond this, as mentioned in Section 3.1, we demonstrate the presence of higher order afterpulses for the first time. We attribute this to the use of the cross-correlation ($g^{(2)}$) between the emission of a photon and all the subsequent APD signals, which allows us to analyze higher order afterpulses.

We can clearly observe the higher order afterpulses in one make of detectors (Excelitas) we tested (see Figure 3.10). Counter-intuitively, detectors with highest afterpulse probability (Laser Components) does not exhibits any higher order afterpulses. We came to conclusion that the presence of higher order afterpulses might be linked to the dead time of the detectors. Unlike, the other two make of detectors (PerkinElmer & Laser Components) the Excelitas SPCM-NIR detectors has the shortest dead time ($\approx 20\,\text{ns}$), whereas in the other two manufacturer have dead times of $\approx 50\,\text{ns}$.

Also, as mentioned in Section 3.4 it should be stressed again that the afterpulses (and higher order order) are more dependent on the electronic quenching circuit of detector rather than on the semiconductors band structure. This might also explain the appearance of higher order afterpulses only in this specific type of detectors.

# Chapter 4

# Variation of afterpulses

In this chapter, we provide a detailed analysis of afterpulsing effect for several different repetition rates (all far from detector saturation) of the laser pulses, detected photon per pulse (we refer to it as DPPLP) and polarizations. The motivation for this study presented in this section is two-fold. We want to minimize systematic error in our measurements and pursue a quantitative comparison while investigating afterpulsing models. It is important to note that although all these studies [14, 16, 46] show equally compelling evidence for their models, they have only performed their experiments using a certain laser pulse repetition rate, detected photon per laser pulse or even on one specific detector. For carrying out a complete investigation of afterpulses, all these parameters needs to be taken into account.

In this chapter, we provide a complete study of afterpulsing behaviour in several makes of detectors (Excelitas, PerkinElmer and $\tau$-SPAD-fast), using all known standard models (power model, hyperbolic sinc model or multiple exponential model) while varying various parameters like laser pulse frequency, DPPLP or even polarization that could potentially affect the afterpulsing behaviour.

## 4.1 Frequency variation

A potential influence of the laser pulse frequency on afterpulses has been so far neglected or taken as granted of have no effects. Measuring the afterpulsing behaviour for several different repetition rates of laser pulses one helps us to rule out systematic errors that we might have in our experimental observations. Most previous studies [4, 16, 54] have concentrated on modeling afterpulses using a particular repetition rate for their laser pulses.

We use a function generator to trigger our 798 nm laser. The laser generates the optical pulses with the set repetition rate. Before we can perform the actual measurement,

we have to ensure having matching conditions e.g. constant background count rate, constant DPPLP and same polarization throughout all measurements, ..

As mentioned in Section 3.2, we use Neutral Density (ND) filters to attenuate the laser pulse and control the number of detected photon per laser pulse. We wanted to perform the whole experiments around a single-photon level, that is why we chose a DPPLP value of 0.75 for this experiment. The selected DPPLP value corresponds to an average photo number of 1.5 per laser pulse. By using a beam splitter while simultaneously performing the measurements, we were able to monitor the DPPLP values using the other output port of the beam splitter.

Furthermore, we also wanted to make sure that the laser pulse is not too bright, which would skew the afterpulse probability computation. Due to twilighting effects and a finite detection efficiency in the dead time" would a brighter pulse result in a broader single peak in our $g^{(2)}$ histogram. We found out that a DPPLP value of 0.75 does not have any broadening effect in our $g^{(2)}$ and it is sufficient to perform our experiement.

Next, since we expect the afterpulsing probabilities ranging from 0.1 % to 10 %, we have to collect a significant amount of data to even encounter marginal changes of some ppm in the afterpulse probability. We decided to run the experiment until we have $200 \times 10^6$ detection events in the APD.

We run each of our measurements for all 3 makes of detectors (PerkinElmer SPCM-AQ4C, Excelitas SPCM-NIR and Laser Components $\tau$-SPAD-fast) multiple times while using more than one function generator, time tagging module and certainly various individual detector of the same kind. These steps allow us to rule out most sources of systematic errors and environmental errors (external conditions affecting the experimental setup) e.g. temperature fluctuations in the laboratory, stray light reaching the APDs and skewing our results.

In case of the SPCM-NIR detectors, we varied the frequency in step of 100 kHz up to 1.2 MHz. We wanted to chose a region where we are far from any malfunctioning behaviour of the detector due to saturation effects. As despicted in Figure 4.1 we observe a clear trend of decreasing afterpulsing probabilities with higher laser frequency. One can clearly see in Figure 4.1 that almost all data points agree with the fit within the $\pm$ 3 standard deviation range with the fit. A possible variation in afterpulse probability due to the laser frequency can not be denied. These changes in afterpulse probabilites are beyond any statistical fluctuations and further investigation is needed.

Additionally, by visually overlapping multiple histograms of different laser frequencies, we also checked if we note any changes in timing structure of the afterpulse tail. At first sight, we do not see any irregularity in the afterpulse tail and assumed to have no differences at all. However, in a close up we do discover changes in the afterpulse tail. Although these changes at a particular time in the afterpulse tail does not look

so significant, it gains enormously in importance while computing the total afterpulse probability. The total afterpulse probability is computed by integrate over the whole duration of the prolonged tail of the afterpulse peak.

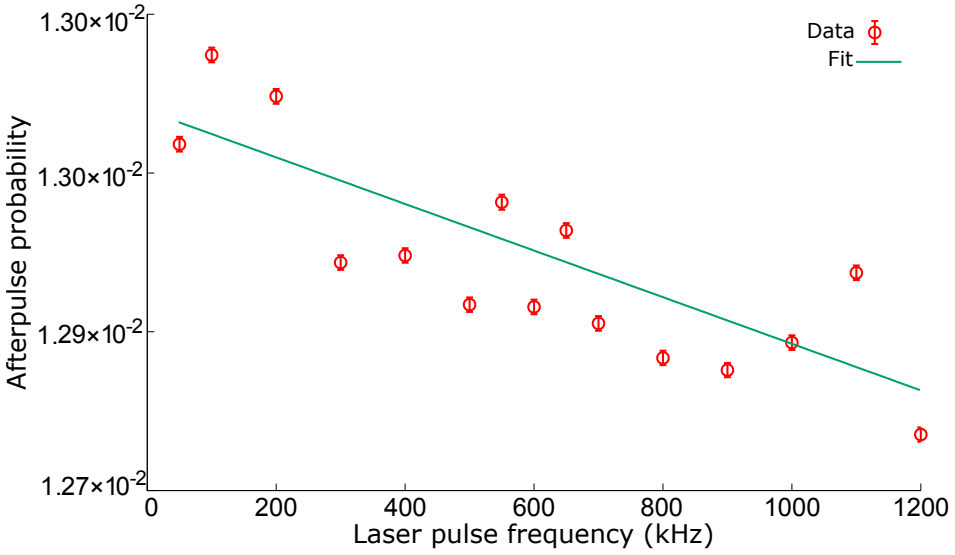


**Figure 4.1:** Total afterpulsing probability in an Excelitas SPCM-NIR detector for different frequencies (50 kHz up to 1.2MHz). The measurements were taken under same conditions such as number of incident photons per laser pulse, background counts, etc. We chose a DPPLP value of 0.75 to perform this experiment. The intensity was kept constant over the whole duration of measurement. We fit the data obtained using the linear regression approach (solid line). We observe a variation in the afterpulse probability due to the laser pulse frequency.

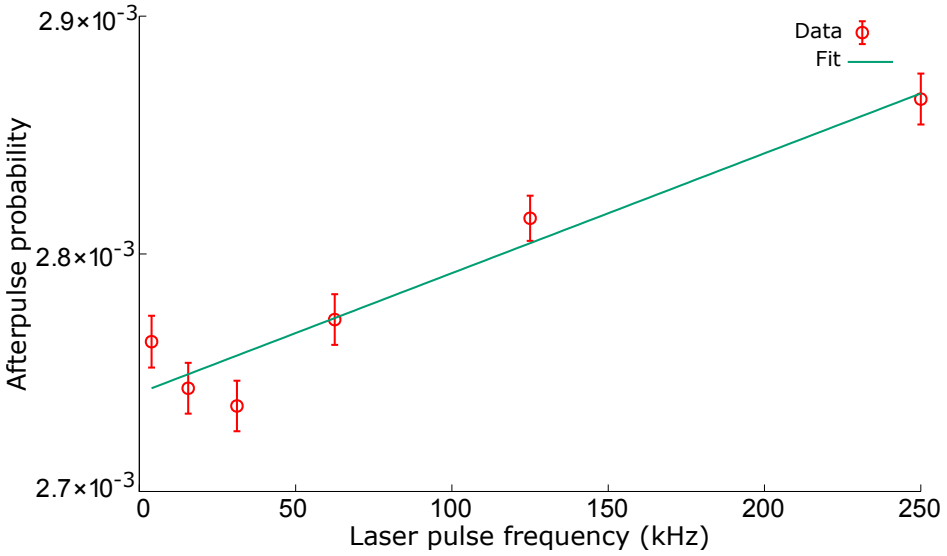


**Figure 4.2:** Total afterpulsing probability in a PerkinElmer AQ4C detector for several different repetition rates of the laser pulses ranging from 3 kHz to 250 kHz (all far from detector saturation). Here, we chose a DPPLP value of about 0.9 and do find significant a variation in afterpulse probability due to laser pulse frequency.

Compared to Excelitas SPCM-NIR the PerkinElmers AQ4C detectors are consist of an older electronic circuit. This might be also the reason, why it saturates at lower count

rates of roughly 1 MHz. Hence, we tested these type of detectors at several different repetition rates ranging from 3 kHz to 250 kHz. Thus, we are operating at low frequencies, we decided to chose an intensity of about 90 % for the sake of a faster data collection. Again, also in this case the total afterpulse probability does show laser frequency dependence and most of the data points are within ± 2 standard deviation limits for statistical fluctuations agree with the fit. In contrast to results in SPCM-NIR in our PerkinElmer AQ4C detector, we have a steady rise with increasing repetition rates.

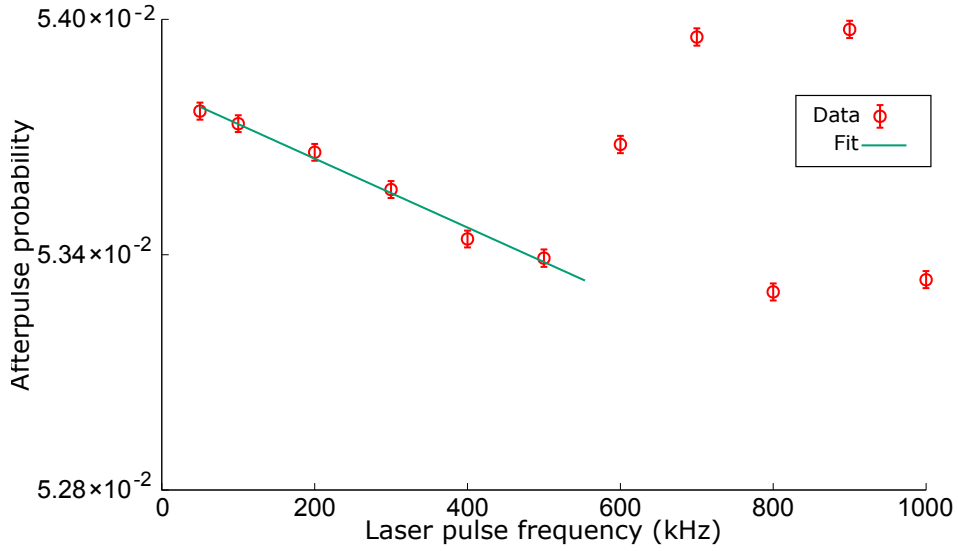


**Figure 4.3:** Total afterpulsing probability in a Laser component $\tau$-SPAD-fast detector for different frequencies (50 kHz up to 1.2MHz). All these frequencies are far from detector saturation. Using the linear regression approach (solid line), we were able to find a fit in the region (50 kHz up to 500 kHz) that agrees to the measured data within 1 standard deviation. In order to obtain a good fit, we had to ignore the data points above 500 kHz.

In case of Laser Components $\tau$-SPAD-fast detectors, we measured a large discrepancy in total afterpulse probability of 5,1 % and 8,5 % between 2 individual $\tau$-SPAD-fast detectors as mentioned earlier in Section 3.4. So, it is of a substantial interest to test these detectors for frequencies variation and see if we also detect any additional dissimilarity in this particular cases. These afterpulse probabilities in $\tau$-SPAD-fast detectors just mentioned are significantly higher compared to other detector makes we tested (e.g. approximately two magnitudes higher than in PerkinElmers AQ4C $\approx$ 0.3 %). Therefore an occurrence of a frequency variation would be easier to detect it in a detector with higher afterpulsing probability. As one can clearly see from Figure 4.3 also in these detectors, we have some laser frequency dependence, especially in the region below 500 kHz.

In all previous works [14–16, 55–57] to date, each paper has used one fixed repetition rate to characterize the afterpulsing behaviour of avalanche photodiodes. Worryingly, a potential influence of the laser pulse frequency on the afterpulse has not been investigated and considered as self-evident to have no effects on the afterpulses. We are the first to measure various repetition rates and detected a dependence between afterpulse probability and the repetition rate of the laser pulses.

From Figures 4.1, 4.2 and 4.3, we can clearly see that afterpulse probability changes with the laser pulse frequency. Judging by the experimental data for all 3 manufacturer, we can report to have a linear response between the afterpulse probability and the laser pulse frequency.

After a thorough investigation of multiple histograms of different laser pulse frequencies (initially visually superimposing and comparing the fitting parameters), we verified that neither the shape, steepness nor duration of afterpulse tail changes. Nevertheless, the total afterpulse probability does change. The change in afterpulse probability is in the magnitude of $10^{-4}$, which is a magnitude lower than variation in afterpulse probability occurring due to polarization and two magnitudes lower than for number of incident photons per laser pulse. Yet, the study of afterpulse probability variation due to the laser pulse frequency is sigificant and important enough to warrant further this study.

## 4.2 Variation with number of incident photons per pulse

As described in Section 3.2, we measure the afterpulse probability of our PerkinElmer APDs using a procedure similar to the setup in Figure 3.1. Unlike the other two free-space detectors (SPCM-NIR and $\tau$-SPAD-fast) our PerkinElmer AQ4C are fiber coupled detectors. The setup to perform the experiments was slightly modified. The attenuated light was fiber coupled instead of being focused onto the active area of the detector. In case of our fiber coupled detectors, the attenuated light after the ND filters has to be first coupled into a singlemode fiber before attaching the fiber onto the APD.

This experiment is performed with a fixed laser repetition rate far away from the saturation region of our detector. We chose a repetition rate of 250 kHz and 500 kHz to have a significant amount of counts stemming from our laser, while investigating the afterpulses when varying the number of detected photon per laser pulse. Additionally for a good signal to noise ratio, it is of a great interest that counts stemming from the laser are higher than the background counts, especially in case of very low DPPLP. For Example, in case of a DPPLP value of $\approx 0.01$, we would end up with an average of 2500 photons/s, while having background counts of $\approx$ 220 photons/s in our PerkinElmer AQ4C detectors.

Next, to prevent damaging the detector by sending too bright pulses, we start our measurement with high ND filters to attenuate the laser to a single photon level or even below. The ND-12 filters were even sufficient to reduce our laser to an average number of a DPPLP value of $\approx 0.01$. Than, we removed ND filters step by step to get to an average of a signal photon detection per laser pulse (corresponding to DPPLP of 1).

The final step was to monitor the intensity before running the actual measurement. Knowing the beam-splitter's ratio and the incident power, we could calculate the intensity in the other output port of the BS used for detection. We monitored the the intensity before, during and for cross-checks also after the measurement. Further, to guarantee having a constant detected photons per laser pulse, we monitored the DPPLP over a considerable amount of time before performing the next measurement.

Initially, we performed the experiment with a repetition rate of 250 kHz and in steps of 0.1 DPPLP from 1 downwards to 0.01 of detected photons per laser pulse. After seeing a trend, we continued in fine steps near that values along with a higher repetition rate of 500 kHz up to a DPPLP value of 0.0025.

Measuring with a different repetition rate is a useful cross-check to see if the repetition rate does influence our results or we obtain a coherent result for both cases. Yet again, we also processed the data with different bin widths to ensure that the observed afterpulse probabilities are not skewed due to any digitization noise.

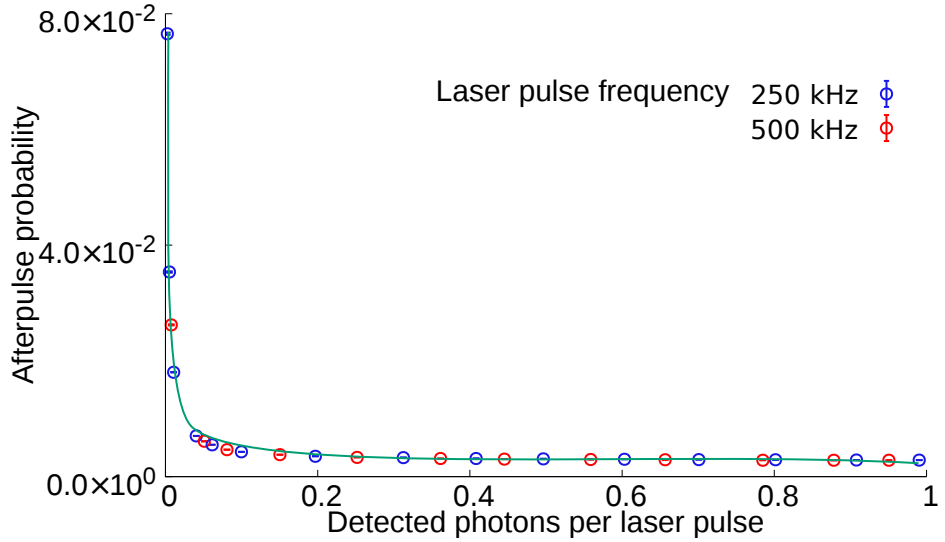


**Figure 4.4:** Afterpulse probability of a PerkinElmer AQ4C detector for various DPPLP values (0.0025 - 0.99). We can observe a uniform afterpulse probability from a DPPLP value of 0.2 up to 1. For lower DPPLP values (0.0025 - 0.2) we can clearly see an exponential decrease of afterpulsing probability for two different laser pulse frequencies (250 kHz and 500 kHz).

One can clearly see in Figure 4.4 that in case of PerkinElmers AQ4C there is a drastic increase in total afterpulsing probabilites for DPPLP values below 0.20. The 0.01 DPPLP measurement has a magnitude higher afterpulsing probability compared to the uniform afterpulsing probability in a region $\geq 0.20$ value. To ensure that our results are not skewed by an individual "faulty" measurement or detector, we not only tested at least 2 individual detectors of same kind but also performed numerous measurements in the regions below 0.1 DPPLP.

Moreover, by visually superimposing multiple histograms of different DPPLP measurements, we verified that neither the shape, steepness, duration of afterpulse tail nor the

timing structure of the signal peak changes. However, we detected a higher signal to noise ratio in our histograms (data fluctuation) due to more accidentals. By using the accidentals correction technique, which can easily correct for higher accidentals (see Section A), we made sure that these counts do not skew our results.

The results of the detected photon per laser pulse variation measurements for Excelitas SPCM NIR detectors are shown in Figure 4.5. While varying the DPPLP values from 1 to 0.01, we kept the laser pulse frequency of 1 MHz and varified having a constant background counts. It can be seen that the afterpulsing probability follows the same trend we already noticed in PerkinElmer detectors. Again, we have a significant variation in total afterpulse probability with decreasing DPPLP values. Although the results are not as drastic as in previous detector (see Figure 4.4) nevertheless it is beyond any statistical fluctuations and can not be ignored in case of a complete afterpulsing study.

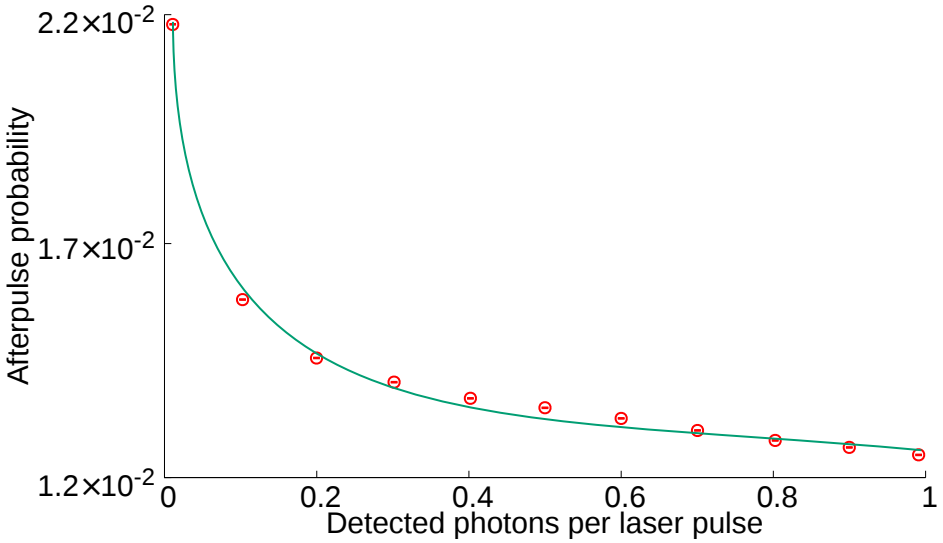


**Figure 4.5:** Afterpulse probability for different DPPLP values in a Excelitas SPCM NIR detector. We detect a significant change in afterpulse probability especially at the single photon level and below ($\leq$ 0.5 DPPLP).

Next, we evaluate the DPPLP variation measurement of our $\tau$-SPAD-fast detectors. We tested three individual $\tau$-SPAD-fast detectors and observed same afterpulsing-intensity behaviour as shown in Figure 4.4 and 4.5. Again, we performed the measurements in steps of 0.1 DPPLP. Unlike SPCM-NIR or SPCM-AQ4C, from Figure 4.6 one can clearly observe a linear change in afterpulse probability. We emphasize that all measurements for these $\tau$-SPAD fast detectors were performed under similar conditions. This interesting avenue of afterpulsing variation due to DPPLP values need a further exploration.

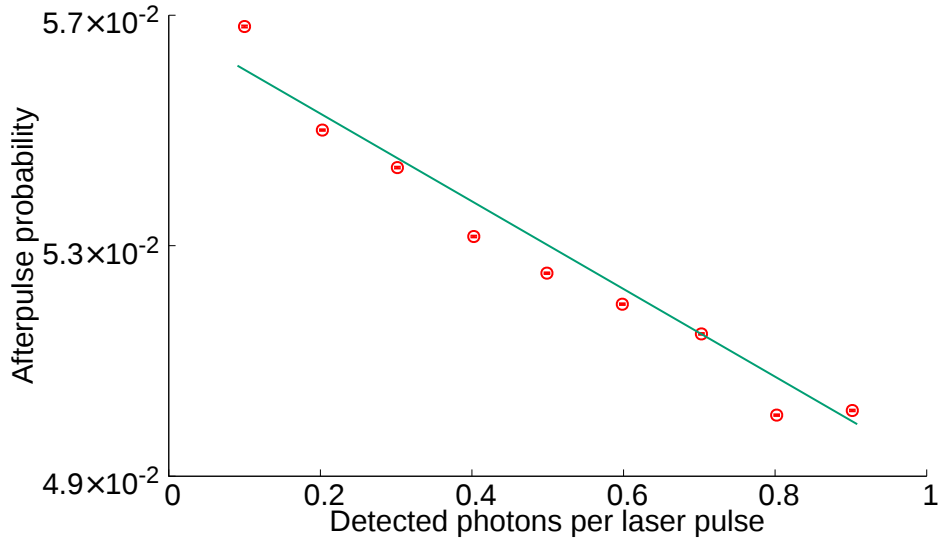


**Figure 4.6:** The DPPLP variation measurement of our $\tau$-SPAD-fast detectors. We see a steady decrease in afterpulse probability for higher DPPLP values. We see a total change of about 1% in afterpulse probability for DPPLP values 0.1 to 0.9. An investigation in region below DPPLP values of 0.1 might reveal an even higher discrepancy in afterpulse probability.

## 4.3 Polarization variation

We implement this polarization variation measurement using the following setup (see Figure 4.7). The experimental setup consists of an input light beam which we thoroughly investigated being almost perfectly linear polarized light source. The first polarizer only allows one polarization to pass through. A Quarter Wave Plate (QWP) placed after the motorized ND filters ensures a circular input polarization. We use the second polarizer placed after the QWP to control the light beam polarization. This allows us reliable measurements in any polarization angle.

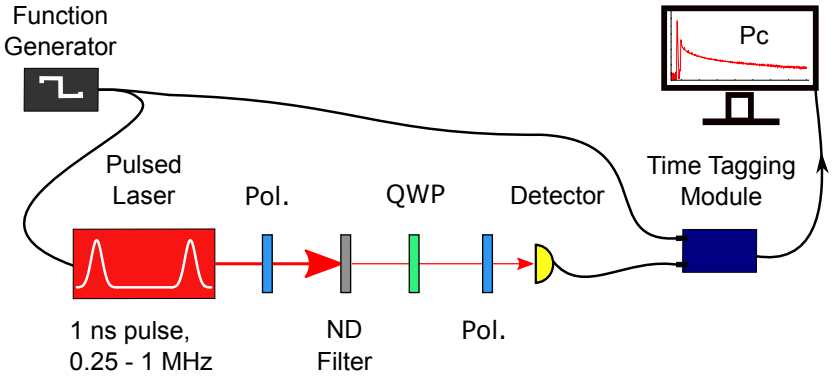


**Figure 4.7:** The experimental setup showing the 798 nm laser that is used to generate pulses with a 1 ns pulse width and 1 MHz repetition rate. The Polarizer (Pol) let uns control the input polarization for the measurement. The Neutral Density (ND) filters are used to attenuate the laser pulse and control the number of detected photon per laser pulse in the APDs. The Quarter Wave Plate (QWP) is used to ensure a circular input polarization.

The motorized ND filter in our setup can deflect the laser beam to hit another section of the active area of our $\tau$-SPAD-fast detectors. It is important to focus on the same area, if we do not have an uniform detection efficiency over the whole active area of the detector.

Using our laser beam with a diameter of $\approx 100\,\mu$m, we were able to scan over the $500\,\mu$m active area of our detector (see Figure 4.8). We used a beam profiler to check for the beam diameter. We started at the center of the active area (referring to 0) and moved the detector in steps of $50\,\mu$m.

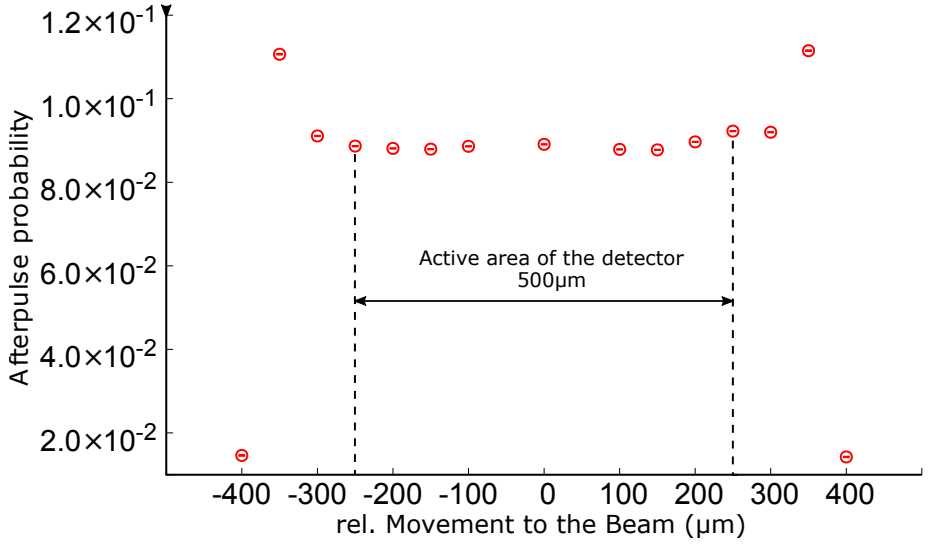


**Figure 4.8:** Scan over the $\tau$-SPAD-fast detectors active area

As we can see from Figure 4.8, we have nearly an equal afterpulse probability over the whole region of the active area. The higher afterpulse probability at the shaded area ($\pm 300$ to $350\,\mu$m) may be explained by the DPPLP dependency of the afterpulses (see Figure 4.6). For Example the DPPLP values at $\pm 350\,\mu$m are at 0.01 and 0.02. These low DPPLP values are not an artifact of higher attenuation by using more ND-filters or using the previously mentioned tilting mechanism. It is a results of only a small fraction of our $\approx 100\,\mu$m laser beam hitting the edge of the active area. During our experiments, while tilting the ND-filters, we made sure to keep the DPPLP values constant and also be well within the active area of the detector. Therefore, we want to stress again that these variation in afterpulse probability are not due to any alignment issues.

Additionally, to avoid as much interference as possible with the experimental setup, we mounted the the QWP and the second polarizer on a stepper motor. We operate both optical elements with a remote control, while the whole setup is covered with a black cloth to keep it under similar conditions. We had a homogeneous background counts though out the duration of the experiment.

Furthermore, due to a laser pulse frequency and DPPLP dependence in all 3 detector makes, we have to make sure to have a constant laser pulse frequency and DPPLP while

performing our polarization variation measurements. As shown in Section 4.1 & 4.2, we observe a significant change in total afterpulsing probability, therefore small flucations in laser pulse frequency or DPPLP can skew our results.

To monitor the DPPLP in the particular detector, we took 5 sets of data every 10 mins before the actual experiment. These preliminary experiments serves not only to determine the DPPLP value [1] but also check for the stability of the DPPLP over periods of time we are going to perform our experiment.

The DPPLP value was chosen based on the afterpulsing response function to the DPPLP (see Figures 4.4, 4.5 & 4.6). We wanted the value to be at a region where the effects of DPPLP on afterpulses are at minimum or preferably non-existent.

Before the polarization variation measurement, we estimated amount of required data to be able to observe any potential changes in the total afterpulsing probability due to polarization. For this purpose, we came to conclusion that $200 \times 10^6$ detection events were sufficient to see changes of the magnitude of $10^{-5}$. Additionally, for each polarization setting, we collected at least 10 sets of data.

For consistency, all measurements were performed with a similar setup shown (Figure 4.7), we switch from our fiber-coupled PerkinElmer AQ4C detector to a free-space one

In order to examine a potential polarization dependence in PerkinElmer detectors, we chose a DPPLP value of $\approx 0.20$. This DPPLP value is located in a plateau region, where the total afterpulse probability is insensitive to small fluctuations in DPPLP (see Figure 4.4). A DPPLP value of 0.2 corresponds to a mean photon number of 0.4 per laser pulse. It is a good trade off between being at the single photon level while avoiding any undesirable effects due to low DPPLP values.

We varied the polarization in step of 10° from 0° to 360° and took 3 data sets for each polarization setting. In between the data sets we realigned the setup to aviod a position dependence. As shown in Figure 4.9, we do not observe any trend nor could we reproduce any of the results with other detectors. Having all 3 data sets superimposed, we only see statistical fluctuations, therefore we conclude that there is no polarization dependence in AQ4C detectors.

Next, we use the same setup as used for PerkinElmer detectors (see Figure 4.7) to test our $\tau$-SPAD-Fast detector for any polarization variation. Unlike PerkinElmer detector it is difficult to find an optimal DPPLP value to conduct this particular experiment. Contrary to PerkinElmer detectors, in $\tau$-SPAD-fast detectors the afterpulse probability

[1] The detected photon per laser pulse (DPPLP) value is dependent on the detection efficiency of the detector. Since there is a significant differences between manufacturers and even between seemingly identical detectors of the same make and batch suggest that every individual detector needs to be calibrated.

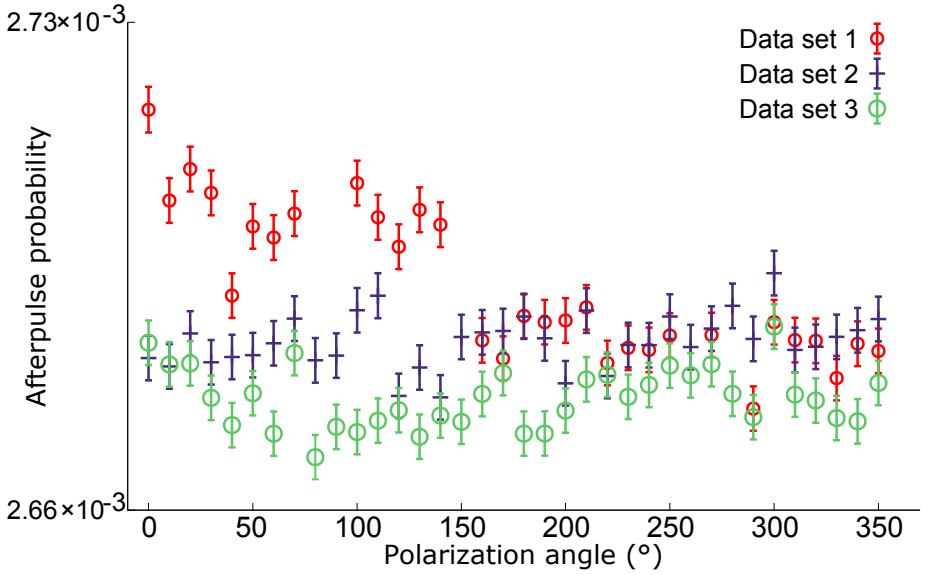


**Figure 4.9:** Afterpulse probability in PerkinElmer AQ4C detectors for various input laser beam polarizations. We varied the polarization in step of 10° from 0° to 360° and took 3 data sets for each polarization setting. We do not any afterpulse probability variation due to the input polarization.

as function of DPPLP behaves differently. We do not have any plateau region where the afterpulse probability is uniform (as shown in Figure 4.6). The afterpulsing response function to the DPPLP for a $\tau$-SPAD-Fast detector is steep for values below 0.4. In this region (DPPLP $\leq 0.4$) the afterpulse probability is more sensitive to slight fluctuations in DPPLP. This could skew our results and therefore we eschew using the same DPPLP value of 0.2 also for this particular type of detectors. We select a DPPLP value of 0.4 to test our $\tau$-SPAD-Fast detectors.

Further, we wanted to keep our DPPLP value as constant as possible, so that it does not skew our polarization measurements. Since imperfection in optical components e.g. QWP or polarizer cause a inconstancy in DPPLP values, we used the ND-filter in our setup to correct for these effects. The ND filters are placed perpendicular to the propagation direction of the laser beam. By mounting the ND filters on a motor, we were able to change their angle with respect to the laser beam. Since the attenuation of the ND filters is dependent on their thickness and consequently their angle, we were able to compensate for the changes in DPPLP.

The approach was to change the polarization in steps of 10° and move the ND filter in fine steps to achieve an equal DPPLP values for each measurement. Data for multiple runs were taken after we have accomplished a stable DPPLP value of $0.400 \pm 0.004$ for each measurement (see Figure 4.10).

From Figure 4.10, we see a sinusoidal behaviour with 90° periodicity. It looks like we might have a polarization dependence in our $\tau$-SPAD-fast detectors. The discontinuity at the values around 100° can be due to simply dust on the polarizer. To confirm our results of the polarization dependency of afterpulsing and additionally investigate the

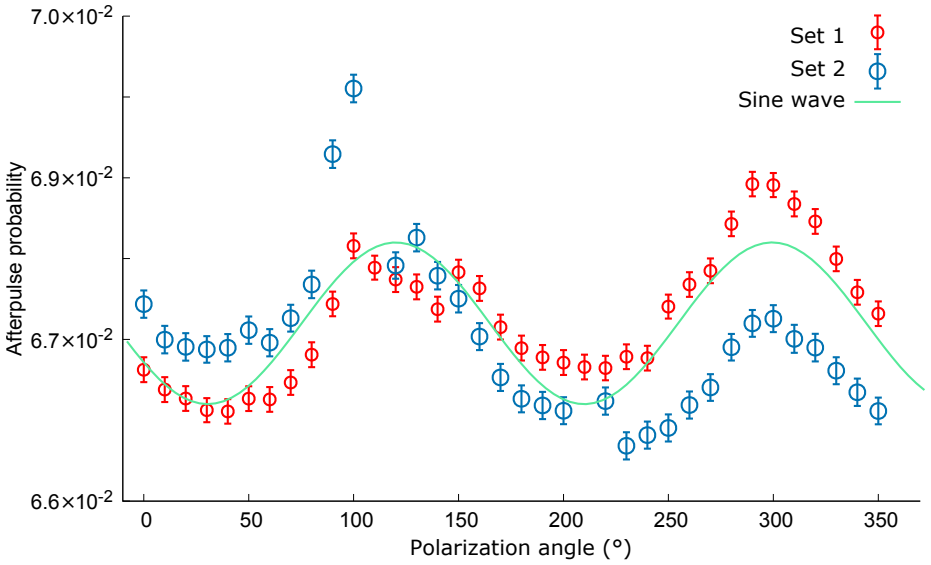


**Figure 4.10:** Afterpulse probability measurement for different input laser beam polarizations in $\tau$-SPAD-fast detectors. We collected in step of 10° from 0° to 360°. The measurements were taken under same conditions such as DPPLP values, noise count rate, etc. In both data sets, we can clearly observe a change in the afterpulse probability. The values obtained for the afterpulse probability for each polarization were fitted to a sine wave. We suspect these changes in the afterpulsing to be due to the polarization.

region around 100°, we took additional 10 individual measurements for each setting, while also realigning the setup in between to avoid any position dependence. Judging by the Figure 4.10 & 4.11, we suspect that indeed an polarization dependence might exist and a further investigation is needed.

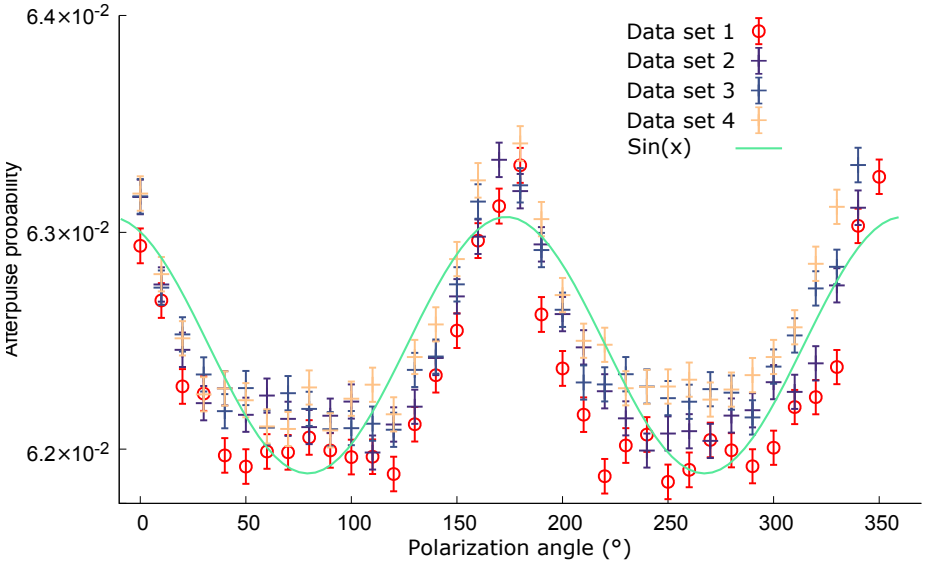


**Figure 4.11:** Polarization variation measurement of $\tau$-SPAD-fast detectors. Again, we observe a sinusoidal behaviour with 90° periodicity. For the sake of clarity, we only plot 4 of total 10 data sets, however the remaining sets follows the same trend.

For our Excelitas SPCM-NIR detectors, we used a more simplified version of our setup

to perform the experiment. After a thorough examination of our light source output, we were able to measure a visibility of 98 % in the two bases (horizontal/vertical). For our first of kind and preliminary investigation we used only a half wave plate $\lambda/2$ to rotate the polarization and have reliable measurements in two complementary bases (e.g. horizontal/vertical) and check of a potential polarization variation. Like the measurements for our $\tau$-SPAD-fast have shown (see Figure 4.6), it is sufficient to measure in two complementary bases to initially check for a potential polarization variation in afterpulses.

Further, we achieved to have a stable DPPLP value of $0.89 \pm 0.08$ throughout our whole experiment for our Excelitas detectors. In this detector, we do not see any significant difference in afterpluse probability due to polarization. We measured a total afterpulse probability of $1.180 \pm 0.005 \times 10^{-2}$ on average when operating in horizontal bases and $1.178 \pm 0.004 \times 10^{-2}$ in vertical.

Our experimental implementation demonstrates for the first time a potential polarization-afterpulsing dependency in single photon detector. We were able to see a sinusoidal behaviour in afterpulse probability with a periodicity equal to 90° in our Laser component $\tau$-SPAD-fast detectors. We however, we were unable to duplicate those results with the other two make of detectors (PerkinElmer SPCM-AQ4C and Excelitas SPCM-NIR).

We note that it is possible to explain the absences of a polarization variation in PerkinElmer SPCM-AQ4C and Excelitas SPCM-NIR detectors due to there much lower afterpulse probability compared to the $\tau$-SPAD-fast detectors. The afterpulse probability of an SPCM-AQ4C detector ($\approx$0,2%) is more than a magnitude lower than $\tau$-SPAD-fast detectors ($\approx$8,5%), therefore it is great challenge to observe these marginal variations in afterpulse probability. Furthermore, the dissimilarity in semiconductor diodes used in the APDs could be also a reason for not observing the same results.

To conclusively affirm our hypothesis of a afterpulse probability variation due to the polarization, a further investigation in this interesting avenue is needed.

## 4.4 Discussion

The results presented in Section 4.1, 4.2 & 4.3 clearly shows a variation in afterpulse probability due to laser pulse frequency, DPPLP values and incident photon polarization. As already pointed out, afterpulses can result in an overestimation of the total count rate by up to 10% and depending on the application of the detector used, it has different implications. However, in many cases these ill effects can be corrected for in post-processing. Nevertheless, a variation in afterpulses probability (e.g. a magnitude higher afterpulse probability for low DPPLP values) can cause major issues and have fatal consequences.

### 4.4.1 Origin of afterpulse variations

Our study of investigating afterpulse variation is first of its kind and therefore the actual cause is not yet well clarified. However, depending on the variation (laser pulse frequency, DPPLP or polarization), we believe to relate these alteration in afterpulse probability to some reasonable physical phenomena. We hope that our results and description of afterpulse variation will be helpful and thought-provoking impulse for future studies on afterpulses.

In case of the frequency variation, we note a linear relationship exists between the afterpulse probability and the repetition rate of laser pulse. Various studies on avalanche photodiodes have already disclosed in the detail the anomalies of these detectors due to the optical pulse frequencies. It is well known that operating the APDs above or at certain repetition rate they suffer from several malfunctioning effects (e.g. saturation effects or blinding mechanisms). Therefore, it is not so improbable to believe that these variation in afterpulse probability due to the laser pulse frequency might be a results of malfunctioning electronics and quenching circuit of the detector.

The potential afterpulse variation due to the input laser beam polarization we noted in our $\tau$-SPAD fast detectors (see Figure 4.10) is the first time to be shown in a single photon counting avalanche photo diode. Here, we speculate that there might be an afterpulse variation due to the polarization of the input laser beam hitting the active area of the detectors. Incident photons with various polarization might have a different influence on the process of depopulation in solids or other underlying mechanism based on fundamental semiconductor physics.

One could argue that the results observed for different input laser beam polarization in our free-space detectors might be influenced by the shielding glass in front of the active area of the detector and therefore skew the photon statistics. However, it should be stressed that only the afterpulse probability varied, while the total counts throughout the entire measurements induced by the incident photons were constant. We did not observe any changes in the total counts due to different input polarization, we can conclusively rule out any the influence of the shielding glass.

The variation in afterpulse probability due to DPPLP appears to be inconsistent with the fundamental understanding of incapability of avalanche photo diodes to resolve the number of photons in an incident laser pulse or in a short time interval. This would mean that independent of the number of photons per laser pulse, there is only one detection event (along with a statistically correlated afterpulse) per pulse. From Figure 4.4 , 4.5 & 4.6 one can clearly observe that the afterpulse probability decreases with higher DPPLP values. This would indicate that the APD can distinguish between several number of photon per laser pulse.

We suspect that the number of incident photons per laser these subsequent photons [2] has an affect on underlying mechanism within the semiconductor or electronic of the detector.

In order to understand our explanation let us briefly look at the the working principle of the p-n junction. As already mentioned in Section 2.4.1, after the initial detection event [3] the detector has a dead time. In this dead time region, although all subsequent photons hit the active area of the detector, its electronic circuit is incapable of detecting any further incident photons.

We assume that higher number of incident photons per laser pulse enhances the sweeping effect of the semiconductor's PIN structure. We suspect that a higher number of photons per laser pulse forces more carriers to decay simultaneously or alternatively faster (in the dead time period). Under such conditions the probability of an afterpulse occurrence is suppressed by the DPPLP value (as shown in Figure 4.4 , 4.5 & 4.6).

The exponential nature of this variation due to number of incident photons per laser pulse can be explained by looking at probabilities for having more than one photon per laser pulse for various DPPLP values we used in our experiment. Unsurprisingly, using the Poisson distribution to estimate the probabilities for having more than one photon per laser pulse, we observe an exponential behaviour with higher number of incident photons per laser pulse. We can conclude that depending on type or sweeping effect in the semiconductor diodes used in the APDs and the number of the incident photons per laser pulse the variation in afterpulse probability has a different exponential behaviour.

To conclusively affirm our hypothesis of the suppression of afterpulse probability due to higher number of photons per laser pulse, a further investigation of afterpulses using Fock states would be interesting. In contrast to our approach of using average photon number per laser pulse, in Fock states (also called number states) we have well-defined number of photons. Intuitively questions that arise are – how the afterpulses behaviour changes when we always have exact one photon per laser pulse (e.g using an entangled pair source in a QKD protocol). How much information can an adversary (Eve) gain about the decoy pulses in a decoy state protocol by just analyzing the variation of afterpulses due to DPPLP values? Besides, this potential side-channel, can the variation of afterpulse due to DPPLP serve as an counter-measurement to detect a blinding attacks [58, 59]?

[2] Here, we mean all photons hitting the active area of the detector during the time period of the dead time and before the detector is reset.

[3] Induced due to an avalanche triggered by an incident photon that creates electrons and electron-hole pairs in the depletion region, just to be swept out of this region to produce a sufficient current to be detected by the APD's electronics.

## 4.5 Conclusion

We demonstrate for the first time the variation of afterpulses for several parameters such as laser pulse frequencies, number of incident photons per laser pulse and laser beam polarization. In particular, our analysis show a linear response of afterpulse probability to the laser pulse frequency in all 3 make/manufacturer of detectors we tested (see Figure 4.3 4.3 & 4.3). For this study, we scanned over a wide range of laser pulse frequency (from 3 kHz up to 1.2 MHz) all far from saturation region of our detectors. Although these changes in afterpulses probability are in the magnitude of $10^{-4}$, one can not deny that we have distinctive results.

As shown in Figure 4.10, we also obtained a potential polarization dependence in one make of detector ($\tau$-SPAD fast). Our results in Section 4.3 explicitly depict that we have a sinusoidal behaviour with 90° periodicity. These variation in afterpulse probability can have devastating consequences in many applicants of avalanche photodiodes. It is especially important for sensitive applicants like quantum key distribution systems when using polarized photons states (quantum channel) to transmit the information and a classical channel to establish secure keys between two parties (Alice and Bob) [60]. Analyzing the transmitted information over the classical channel, the eavesdropper might gain information about the overall statistics of the exchanged key between these two parties.

We strongly believe that afterpulses and variation in afterpulses as a novel discovery, can adversely affect the security of the system hence should be a part of the security analysis of the quantum key distribution system.

Furthermore, also in Life science applications such as Fluorescence Lifetime Imaging (FLIM), Fluorescence Correlation Spectroscopy (FCS), etc., these variation of afterpulses can skew the photon counting statistics. Imaging techniques (FLIM and FCM and many more) are not only based on the concentrations of detected particles (molecules) but also the excitation intensity from a fluorescent. This means that, the polarization or intensity of the emitted photon (originating from the fluorescent sample) influences the probability of the afterpulses and therefore lead to crucial mistakes.

As already mentioned, afterpulse effect can result in an overestimation of the total count rate by up to 10 % and lead to an overestimation of the concentration of fluorophores. The significant variation in afterpulse probability due to DPPLP values we discovered in all 3 make of detectors enhance this effect even further. For example, a dim or a much brighter fluorescent sample would lead to complete different results and therefore contribute to a wrong diagnose.

Furthermore, previous studies have not investigated nor mentioned these variation of afterpulses due to number of incident photon per laser. We are the first to report on

these. Thus, it has not been evaluated to which extent these can affect the security of a quantum quantum key distribution protocols.

We assume that, in a decoy state protocol [61, 62] an eavesdropper could eventually make use of the variation of afterpulses to extract valuable information about the transmitted key. Wang et al. [62] proposed a decoy-state method by using different mean photon numbers way below one (e.g. $\mu = 0.3$ and $\mu' = 0.5$) to overcome the photon number splitting (PNS) attack for BB84 [60] quantum key distribution protocol. However, with the help of variation of afterpulse probability because of the number of incident photons per laser pulse, an eavesdropper might be able to differentiate between signal and decoy pulses. As depicted in Figure 4.4, 4.5 & 4.6, one can easily distinguish different DPPLP values from each other, which might give Eve an edge about the exchanged key.

We also believe that variation in afterpulse probability due to number of incident photons per laser pulse can also have positive side-effects. It can used to detect a blinding attack in a QKD system. By analyzing the afterpulse probability one can spot the bright illumination that is used to remote-control avalanche photodiodes (APDs) such as those described in Refs. [58, 59]. A quick investigation of afterpulse probability can easily reveals the presence of an eavesdropper.

# Chapter 5

# Conclusion and outlook

In this thesis, I have provided a complete study on the afterpulse effect in three completely different type of single photon counting avalanche photo diode detectors. By performing the first comparative study of afterpulsing behavior, we were able to demonstrate that statistically significant different models are required to appropriately describe the distribution of electrical signals generated by different brands detectors. In Chapter 3, we demonstrated that none of the previously reported models applied are universal and hence can not be applied to all the brand/makes of detectors. We show a strong evidence that the characterization of afterpulsing behavior can not be exclusively attributed to the presence and distribution of deep levels in the semiconductor's band structure.

Furthermore, in course of analyzing and pursuing a quantitative comparison while investigating the afterpulse effect, I was able to show two novelties: higher order afterpulses (Section 3.5) and the variation in afterpulse probability due to various parameter such as laser pulse frequency, number of incident photon and laser beam polarization (Chapter 4). To the best of our knowledge, none of these discoverers have ever been reported.

We can conclude, that the basic principles of and physical origin behind afterpulsing are not fully understood and remark that the existing standard models are often too simplistic and do not take include several effects. Thus, we suggest that for an accurate modelling/characterization of the afterpulses, it is sufficient to also include various effects due to the electronics or quenching circuits of the detectors, higher order afterpulses and the variation of afterpulses. We propose that, we have to jettison the idea of having a fundamental model describing the afterpulse all type of single photon counting avalanche photo diode detectors. Therefore, we propose that each individual detector needs a careful calibration before it's use. Especially, in sensitive applicants when performing device-dependent quantum key distribution – in which the two parties use well characterized measurement devices [63].

Beyond this, I would encourage the investigation of this afterpulses in future experiments. For instance, a future iteration of this project could be testing the afterpulse effect in a commercial QKD system. By doing this, we can probe how significant eavesdropper's overall statistical knowledge about the key can be. An advantage of performing the characterization of afterpulse effect in a QKD setup would be to perform a countermeasurement to foil quantum blinding attacks, as demonstrated in Refs. [58, 59].

Furthermore, the significance of variation in afterpulses has not been fully understood nor investigated yet. We suspect that in the context of QKD, this might eventually open up a security loophole and make commercial QKD systems vulnerable for Eve to hack. Thus, for the sake of the security analysis of some systems, we suggest to pursue a deeper analysis of this new discovery.

# Appendix A

# Background and accidentals corrections

In typical quantum optics experiments, there is a probability that the detectors registers photon detection events in absence of a "valid" incident photon from a light source. This might be the result of stray light including black-body radiation or by noise on the electrical signal or just thermal noise [5] It is essential to correct for these false detection events, otherwise these counts induces an overestimation of the count rates and influence the outcome of the measured data and skew our photon counting statistics.

These false detection events are called background and dark counts. Although it is common to use these terms background counts and dark counts as synonymic to each other, we distinguish between both of them. Background counts are due to stray light from external sources hitting/reaching the detector and causing spurious detection events, while dark counts are an artifact of the detectors itself. Dark counts (solely) arise due to electrical and thermal noise. Furthermore, noise counts includes both the dark and background counts together.

In many papers, it has not been seen as compulsory to correct the $g^{(2)}$ histograms for these noise counts. Several previous works have put their efforts into finding a universal and fundamental model of afterpulsing [4, 12–15, 17, 18] rather than computing the actual afterpulsing probability. An additional constant noise count rate does not matter when characterizing the afterpulse behavior and fitting the results to various models. We were also able to verify that the fitting parameter of each of the standard models (see Equations 2.1, 2.3 and Equation 2.6) to our experimental data is independent of the noise counts correction.

However, as mentioned in Section 3.4, to efficiently and accurately perform experiments we must characterize each individual detector. This is especially true for sensitive

applications like quantum communication, because the security of any real world implementation (i.e. with a high transmission loss) depends on the devices used. Hence the precise characterization of the non ideal behavior of single photon detectors (and all other components of the quantum communication device) are critical for practical security proofs.

By correcting for these spurious counts, we are able to distill the actual detection events stemming from the laser pulse, their subsequent correlated afterpulses and consequently obtain an accurate value for the detectors afterpulsing probability.

Usually in quantum optics measurements, there is a probability that a coincidence is detected between two different detectors erroneously, we call these coincidences "accidentals". In our case accidentals are invalid detection events in absence of a real photon been detected by our APDs while there has been a trigger pulse from the function generator to our laser diode. Typically, they can be estimated from Poissonian statistics as: $r_{acc} = r_1 r_2 t_c$, where $r_{acc}$ is the rate of the accidental coincidences, $r_1$ and $r_2$ are the count rates of the individual detectors and $t_c$ is the coincidence time window used [1]. Many experiments simply subtract these estimated rate of accidentals coincidences $r_{acc}$ from their data to correct for it. It is also a common practice to directly computed the rate of accidentals coincidences from the $g^{(2)}$ histogram as previously mentioned in Section 3.2 and corrected for it.

We can conclude that the estimated values (using the formula $r_{acc} = r_1 r_2 t_c$) and the experimentally extracted values from the $g^{(2)}$ histogram agree within 1 standard deviation. We can also determine that simply subtracting the accidental counts may be a good approximation when the detection rates are very low compared to the peak count rate.

However, we identified an irregularity while using this common practice of accidentals correction in the so called "Dead time"[2]. In this section we focus on the effect of the dead time. By varying the background count rates while performing the experiment, we want to investigate the dead time region behaviour of various detectors. Further, we want to check if the common practice of subtracting accidentals counts also hold for high background count rates (up to 250kcps).

We use a battery powered LED as a continuous, steady and controllable source of background illumination in addition to the attenuated laser pulses (see Figure 3.1). We varied the background count rates from 40 kcps to 240 kcps and then measured the $g^{(2)}$ histograms (see Figure 3.1).

[1] In our particular experimental setup, $r_1$ is the count rate from our detector, but $r_2$ the trigger signal from our function generator. Although the formula assumes a Poissonian distribution in $r_1$ and $r_2$ , the trigger signal from the function generator is not Poissonian. Therefore, it is very interesting that the results of the estimated values still matches the experimental data so well.

[2] "Dead time" is a misnomer because the detector is not completely dead/inactive instead it exhibits a reduced detection efficiency.

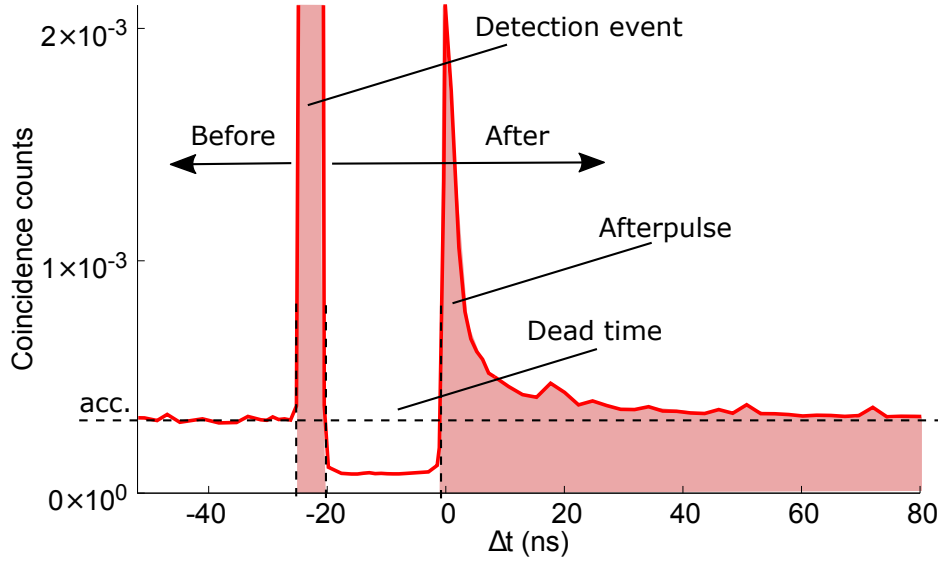


**Figure A.1:** The Figure shows the 3 significant regions, we apply the correction for. We see the region before the detection event, the region shortly after the detection event, where the detectors exhibit a dead time and the region after the detection event. In the dead time region, the detector is not dormant, but we still observe counts with a lower detection efficiency. As a result, we can not correct the whole $g^{(2)}$ using the common practice of just subtracting the accidentals (acc.).

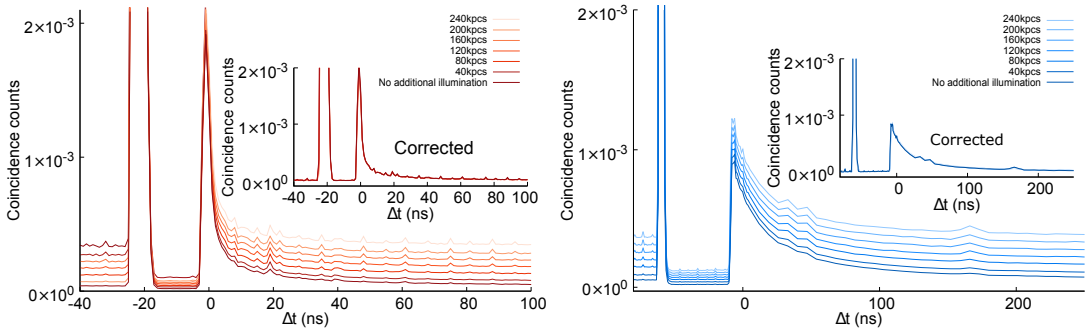


**(a)** Excelitas SPCM-NIR APD module.

**(b)** Laser Components $\tau$-SPAD-fast APD module.

**Figure A.2:** $g^{(2)}$ Histograms for different background count levels, clearly showing the probability of detection events during dead time region (between the large detection peak and time $\Delta t = 0$). We observe a linear scaling of the accidental coincidences as we vary the background count rate. **Insets**: The $g^{(2)}$ histograms corrected for background counts.

We find that in the regions before the detection event, well after the detection event and even during the afterpulse, the corrections provides good results (see Figure A.1). However, in the region shortly after the detection event, where the detectors exhibit a "dead time", the standard correction methods (using poissonian statistic or computing directly from the experimental data to calculate the rate of accidentals) can not be applied. As depicted in the Figure A.1 the accidental level in the dead time region is well below of the rest of the histogram. Therefore, a separate correction for this region is required.

From Figure A.2, we can demonstrate that in the dead time region the detectors are

not completely inactive but the detection efficiency is reduced by a factor $\alpha$ which is characteristic of the detector. We observe a linear scaling of the accidental coincidences as we vary the background count rate. From which we determine the reduction factor $\alpha$ in this dead time region (see Table A.1). We have to modify the $r_{acc}$ equation and include the reduction factor $\alpha$ for the dead time region. Now the accidentals correction can also be applied to the whole $g^{(2)}$ histograms (region before the detection event, well after the detection event, during the afterpulse and now even in the dead time region). Furthermore, the inset of figure A.2 shows that the our corrections are truly background level independent.

| Detector | $\alpha_{avg}$ | $\alpha_{min}$ | $\alpha_{max}$ |
|---|---|---|---|
| SPCM-NIR | 3.97 ± 0.06 | 3.86 ± 0.05 | 4.06 ± 0.20 |
| $\tau$-SPAD-fast | 3.31 ± 0.06 | 3.30 ± 0.07 | 3.32 ± 0.15 |

**Table A.1:** The correction factor $\alpha$ to be applied for the dead time depends on the make of detector. The table shows the average value ($\alpha_{avg}$) as well as the minimum ($\alpha_{min}$) and maximum ($\alpha_{max}$) values as the background level was varied from 40 kcps to 240 kcps. The SPCM-AQ4C is a fiber coupled detector and we could not introduce background light using the LED in the same manner as the other detectors and is omitted from this table for consistences.

# Appendix B

# Cross-correlation source Code

The software is written in Anaconda Python 2.7 for windows. We chose Python because python's syntax is very clear and readable, so it makes easy for us to understand and program. There are various ways to write the code for a cross-correlation function, most probably a much faster way. The next iteration would be to use C, Fortran, C#, etc.

This software only accepts data from the time tagging module (TTM8000) that was measured with the TTM Viewer- Data Source software and converted to "pretty hex" format by the TTM Converter software.

```
1  #this program only accepts data that was measured in the I mode of teh TTM8000 module and was
    ↪  converted to hex format by the bundled software ttmcnvt.exe using the -o h option.
2
3  #the following are the recognised commandline arguments
4
5  # -i input file name should be the the  data file from the TTM8000 module after it has been
    ↪  processed into 'prety hex' format by the ttmcnvt bundled program. This can be done by using
    ↪  the encapsulating python script binTohex_convert.py
6  # -o output file. The outputfile will consist of a 1 line header starting with # The file format
    ↪  will have two columns (space separated) with the first column being the start of each bin in
    ↪  ns and the second being the number of coincidence events that fallinto that bin
7  # -w binwidth in ns
8  # -m maximum time difference for correlation search (max of delta t)
9  # -c channel string. A number corresponding to the channels to use. 01 would mean use channel 0 as
    ↪  trigger and 1 as the signal. simillarly 32 would mean channel 3 is the trigger and 2 the
    ↪  signal. Single digit numbers will be presumed to be preceded by a zero so 04 and 4 are the
    ↪  same
10 # -h Print this help screen
11
12 import numpy as np
13 from os.path import getsize
14 import sys
15 from time import time
16 TTMConvFactor=82.3/1000 #Conversion factor to convert the time interval of the TTM8000 module into
    ↪  ps. This value is taken from the manual. The program uses ns. so we devide by 1000 to convert
    ↪  ps to ns (Assuming I modefor data collection)
17 FileChunkSize=1024 * 1024 * 1024 #If the file is larger than this value (in bytes) then the file
    ↪  will be loaded as smaller chunks of this size.
```

```
18  BytesPerLine=23 #in our defined data format each line consists strictly of 23 bytes each.
19  def int16(x): #This function converts the hexadecimal string in th 0x format to an intiger. This
     ↪  function is used in the call to genfromtxt under converters to directly apply the
     ↪  transforamtion on the data as it isread from the file.
20      return(TTMConvFactor*int(x,16)) #We multiply by the conversion factor directly here such that
     ↪  all values in the program after the genfromtxt command are available directly in ns
21  def filter_lines(f, start, stop): #defining the start and stop points of the chunks for the
     ↪  loadtxt-command
22          for i, line in enumerate(f):
23                  if i >= start and i<= stop :
24                          yield line
25
26
27  progstarttime=time()
28
29  arguments=len(sys.argv)
30  if (arguments<6):
31          print "This program is designed to compute a temporal correlation function for data from
     ↪  the TTM8000 module. The output is a delay histogram. \n\n -i input file name should be the
     ↪  data file from the TTM8000 module after it has been processed into 'prety hex' format by the
     ↪  ttmcnvt bundled program. This can be done by using the encapsulating python script
     ↪  binTohex_convert.py \n\n -o output file. The outputfile will consist of a 1 line header
     ↪  starting with # The file format will have two columns (space separated) with the first
     ↪  column being the start of each bin in ns and the second being the number of coincidence
     ↪  events that fallinto that bin \n\n  -w binwidth in ns\n\n -m maximum time difference for
     ↪  correlation search (max of delta t)\n\n -c channel string. A number corresponding to the
     ↪  channels to use. 01 would mean use channel 0 as trigger and 1 as the signal. simillarly 32
     ↪  would mean channel 3 is the trigger and 2 the signal. Single digit numbers will be presumed
     ↪  to be preceded by a zero so 04 and 4 are the same\n\n -h Print this help screen\n"
32          sys.exit()
33  for arg in range(1,arguments):
34      if (sys.argv[arg] == '-i' or sys.argv[arg] == '-I'):
35          infile=sys.argv[arg+1]
36      if (sys.argv[arg] == '-o' or sys.argv[arg] == '-O'):
37          outfile=sys.argv[arg+1]
38      if (sys.argv[arg] == '-w' or sys.argv[arg] == '-W'):
39          try:
40              binwidth=float(sys.argv[arg+1])
41          except:
42              print "The binwidth must be a floating point number. representing the width of each
     ↪  bin in the histogram in ns"
43
44          if (binwidth <=0):
45              print "The binwidth must be positive and greater than 0 reverting to a default value
     ↪  of 10ns"
46              binwidth = 10
47          if (binwidth > 10000):
48              print "The binwidth must be smaller than 10 micro seconds. Setting it to the max
     ↪  limit"
49              binwidth = 10000
50      if (sys.argv[arg] == '-M' or sys.argv[arg] == '-m'):
51          try:
52              max_delta_t=float(sys.argv[arg+1])
53
54          except:
55              print "The max delta t must be a number"
56
57          if (max_delta_t <=0):
```

```
58              print "The max_delta_t must be positive and greater than 0 reverting to a default
    ↪   value of 1us"
59              max_delta_t = 1000
60          if (max_delta_t > 10**10):
61              print "The max_delta_t must be smaller than 10 seconds. Setting it to the max limit"
62              max_delta_t = 10**10
63      if (sys.argv[arg] == '-c' or sys.argv[arg] == '-C'):
64          try:
65              ch=int(sys.argv[arg +1])
66          except:
67              print "The channel must be a number. Only the first two digits will be considered"
68
69          if (ch > 77 or ch<0):
70              print "Invalid chanel selection there are only 8 channels and only a two or 1 digit
    ↪   positive number is accepted as the channel selection defaulting to 01"
71              ch = 1
72          ChA= int(ch/10)
73          ChB = int(ch -10*ChA)
74          if (ChA >7 or ChB>7):
75              print "There are only channels 0 to 7. Defaulting to Channels 01"
76              ChA = 0
77              ChB = 1
78      if (sys.argv[arg] == '-h' or sys.argv[arg] == '-H' or len(sys.argv)<6):
79          print "This program is designed to compute a temporal correlation function for data from
    ↪   the TTM8000 module. The output is a delay histogram. \n\n -i input file name should be the
    ↪   the  data file from the TTM8000 module after it has been processed into 'prety hex' format
    ↪   by the ttmcnvt bundled program. This can be done by using the encapsulating python script
    ↪   binTohex_convert.py \n\n -o output file. The outputfile will consist of a 1 line header
    ↪   starting with # The file format will have two columns (space separated) with the first
    ↪   column being the start of each bin in ns and the second being the number of coincidence
    ↪   events that fallinto that bin \n\n  -w binwidth in ns\n\n -m maximum time difference for
    ↪   correlation search (max of delta t)\n\n -c channel string. A number corresponding to the
    ↪   channels to use. 01 would mean use channel 0 as trigger and 1 as the signal. simillarly 32
    ↪   would mean channel 3 is the trigger and 2 the signal. Single digit numbers will be presumed
    ↪   to be preceded by a zero so 04 and 4 are the same\n\n -h Print this help screen\n"
80
81  print "\n\nStarted g2 computation with a bin width of ", binwidth," ns \n and maximum time
    ↪   difference to search for of ", max_delta_t/1000 ," us.\n The output will be saved to the
    ↪   file ",outfile, "\n\n Using Channels: ",ChA," and ", ChB
82
83  filesize=getsize(infile)
84  numchunks=1
85  chunksize=int(filesize/BytesPerLine)
86  numlines=float(float(filesize)/BytesPerLine)
87  if (numlines - int(numlines) != 0):
88          print "The data file does not have exactly 23 bytes per line in every line! Undefined data
    ↪   format. Will exit! (remember that the last char in the file should be an end line)"
89          sys.exit()
90
91  if (filesize>FileChunkSize):
92          chunksize=int(FileChunkSize/BytesPerLine)
93          numchunks=int(numlines/chunksize)
94
95  numbins = int(max_delta_t/binwidth)+1
96  print "Numbins=",numbins
97  histo=np.zeros((numbins,2), dtype = float)
98  for i in range (numbins):
99          histo[i,0]=i*binwidth
100
```

```
totchA = 0
totchB=0
datastarttime=0
dataendtime=0
datatimeflag_isfirstchunk=1
for chunk in range(numchunks):
        startline = chunk * chunksize
        stopline = (chunk+1) *chunksize
        if (stopline > numlines):
                stopline=numlines


        with open(infile) as f:
                data = (np.loadtxt(filter_lines(f, startline,stopline), dtype=None, usecols
    =(0,2),converters={2:int16}))
        if (datatimeflag_isfirstchunk==1):
                datastarttime=data[0,1]
                datatimeflag_isfirstchunk=0
        dataendtime=data[-1,1]

        subsetA = data[data[:,0] == ChA][:,1]
        subsetB = data[data[:,0] == ChB][:,1]

        del data
        lenA=len(subsetA)
        lenB=len(subsetB)

        totchA += lenA
        totchB += lenB
        print "Loaded data for chunk ",chunk, " out of ",numchunks, " \n We have ", lenA, " points
    from chA and ", lenB, " points in chB."

        for i in range(0,lenA):
                delta_t = 0
                j = np.searchsorted(subsetB,subsetA[i])
                while (delta_t < max_delta_t and j<lenB):
                        delta_t = subsetB[j] - subsetA[i]
                        try:
                                if(delta_t<max_delta_t):
                                        histo[int(delta_t/binwidth),1]+=1
                        except:

                                print "there was an error assigning histo bin",
    int(delta_t/binwidth), "delta t = ",delta_t, " max_delta_t ",max_delta_t
                                print "histo length",len(histo)
                                sys.exit()
                        j = j+1

                if (i%10**6 == 0):
                        print "Completed processing ",
    (i+(lenA*chunk))/float(lenA*(numchunks+1))*100, ' % of all the data\n'

        with open('temphisto_Chunk{0}.g2'.format(chunk),'w') as temporf:
                np.savetxt(temporf, histo, delimiter= ' ')
with open(outfile,'w') as outf:
        headderstr="# Measurement Duration = "+ str((dataendtime-datastarttime)/(10**9))+ " s\n#
    Total counts in ChA = "+ str(totchA)+ "\n# Total counts in ChB = "+str(totchB)+ "\n# Total
    coincidences between channels "+ str(ChA)+ " and "+str(ChB)+ " is "+ str(sum(histo[:,1]))+
    "\n# StartOfTimeBin(ns)_deltaT CoincidencesPerBin \n"
```

```
153         outf.write (headderstr)
154 with open(outfile,'a') as outf:
155         np.savetxt(outf, histo, delimiter= ' ')
156 print "file written",outfile
157 progendtime=time()
158 print "the program took ",progendtime-progstarttime, " s to execute"
```

# Acknowledgements

First and foremost, I would like to thank Professor Anton Zeilinger for welcoming me into his group and giving me this unique opportunity to work alongside such dedicated and talented scientists.

Thank you to Dr. Rupert Ursin for his constant guidance and support during the past year. His determination to work alongside his students, willingness to share his extensive knowledge, and infinite patience is what fosters growth in philomathic students, like myself. He truly taught me how to think like a scientist and, for that, I am eternally grateful.

Additionally, I would also like to thank my coworkers at the IQOQI, Bo Liu, Dominik Rauch, Evelyn Ortega, Fabian Steinlechner, Farbod Fonoon, Johannes Handsteiner, Lukas Bulla, Matthias Fink, Sebastian Ecker, Sebastian Neumann, Sören Wengerowsky, Thomas Scheidl and Yuanyuan Chen for sharing their knowledge with me. It has been a pleasure and an honor for me to work with such a motivated group of peers..

My most sincere gratitude goes to my adviser and mentor, Dr. Siddarth Joshi. Words cannot describe how often I have inundated him with incessant questions and requests for help while performing my experiment. He selflessly put his own work aside to provide me with direction and advice. Because of his commitment to my success, I have learned how to successfully work in a lab and conduct experiments. His passion for science, dedication to his work, and profound knowledge has influenced and continues to serve as an inspiration to me. It has been such a privilege to learn from you and I appreciate all that you have done for me.

Last but certainly not least, I wish to thank my parents, Shahzia and Abdulwase Ziarkash, for their unconditional love and support; my beloved siblings, Yalda, Muska, Sabawoon, Mina, and Tareq; as well as my close friends for their encouragement throughout all of these years.

# Bibliography


[1] Daniel Gottesman, H-K Lo, Norbert Lutkenhaus, and John Preskill. Security of quantum key distribution with imperfect devices. In *Information Theory, 2004. ISIT 2004. Proceedings. International Symposium on*, page 136. IEEE, 2004.

[2] Daniel Gottesman, Hoi-Kwong Lo, Norbert Lütkenhaus, and John Preskill. Security of quantum key distribution with imperfect devices. *arXiv preprint quant-ph/0212066*, 2002.

[3] Nitin Jain, Birgit Stiller, Imran Khan, Vadim Makarov, Christoph Marquardt, and Gerd Leuchs. Risk analysis of Trojan - horse attacks on practical quantum key distribution systems. *IEEE Journal on Selected Topic in Quatum Electronics*, 21(3): 1077–260X, 2014. ISSN 1077-260X. doi: 10.1109/JSTQE.2014.2365585. URL http://www.ieee.org/publicationsstandards/publications/rights/index.html.

[4] Mark A. Itzler, Xudong Jiang, and Mark Entwistle. Power law temporal dependence of InGaAs/InP SPAD afterpulsing. *Journal of Modern Optics*, 59(17):1–9, 2012. ISSN 0950-0340. doi: 10.1080/09500340.2012.698659.

[5] Siddarth Koduru Joshi. *Entangled Photon Pairs: Efficient Generation and Detection, and Bit Commitment*. PhD thesis, 2014.

[6] Transition edge sensor, 2017. URL https://en.wikipedia.org/wiki/Transition_edge_sensor.

[7] M. D. Eisaman, J. Fan, A. Migdall, and S.V. Polyakov. Invited review article: Single-photon sources and detectors. *Review of scientific instruments*, 82(7):071101, 2011.

[8] Photodiodes and other semiconductor devices, 2017. URL http://unicorn.ps.uci.edu/243/handouts/243Photodiodes.pdf.

[9] Alan Migdall, Sergey V Polyakov, Jingyun Fan, and Joshua C Bienfang. *Single-Photon Generation and Detection: Physics and Applications*, volume 45. Academic Press, 2013.

[10] Andrea Gallivanoni, Ivan Rech, and Massimo Ghioni. Progress in quenching circuits for single photon avalanche diodes. *IEEE Transactions on Nuclear Science*, 57(6 PART 2):3815–3826, 2010. ISSN 00189499. doi: 10.1109/TNS.2010.2074213.

[11] Cross-correlation, 2017. URL https://en.wikipedia.org/wiki/Cross-correlation.

[12] D. B. Horoshko, V. N. Chizhevsky, and S. Ya. Kilin. Full-response characterization of afterpulsing in single-photon detectors. *arXiv:1409.6752 [quant-ph]*, pages 1–4, 2014. URL http://arxiv.org/abs/1409.6752.

[13] A. C. Giudice, M. Ghioni, S. Cova, and F. Zappa. A process and deep level evaluation tool: Afterpulsing in avalanche junctions. In *European Solid-State Device Research Conference*, pages 347–350, 2003. ISBN 0780379993. doi: 10.1109/ESSDERC.2003.1256885. URL http://ieeexplore.ieee.org/lpdocs/epic03/wrapper.htm?arnumber=1256885.

[14] Sergio Cova, A. Lacaita, and G. Ripamonti. Trapping Phenomena in Avalanche Photodiodes on Nanosecond Scale. *IEEE Electron Device Letters*, 12(12):685–687, 1991. ISSN 15580563. doi: 10.1109/55.116955.

[15] Christoph Schaeff Sven Ramelow Mario Stipčevi˜c Gerhard Humer, Momtchil Peev and Rupert Ursin. A simple and robust method for estimating afterpulsing in single photon detectors. *Journal of Lightwave Technology*, 33(14):3098–3107, 2015.

[16] D. B. Horoshko, V. N. Chizhevsky, and S. Ya. Kilin. Afterpulsing model based on the quasi-continuous distribution of deep levels in single-photon avalanche diodes. *Journal of Modern Optics*, 0340(September):1–5, 2016. ISSN 0950-0340. doi: 10.1080/09500340.2016.1220643. URL https://www.tandfonline.com/doi/full/10.1080/09500340.2016.1220643.

[17] K. E. Jensen, P. I. Hopman, E. K. Duerr, E. A. Dauler, J. P. Donnelly, S. H. Groves, L. J. Mahoney, K. A. McIntosh, K. M. Molvar, A. Napoleone, D. C. Oakley, S. Verghese, C. J. Vineis, and R. D. Younger. Afterpulsing in Geiger-mode avalanche photodiodes for 1.06 $\mu$m wavelength. *Applied Physics Letters*, 88(13):10–13, 2006. ISSN 00036951. doi: 10.1063/1.2189187.

[18] Mario Stipčević, Daqing Wang, and Rupert Ursin. Characterization of a Commercially Available Large Area, High Detection Efficiency Single-Photon Avalanche Diode. *Journal of Lightwave Technology*, 31(23):3591–3596, 2013. ISSN 0733-8724. doi: 10.1109/JLT.2013.2286422. URL http://ieeexplore.ieee.org/lpdocs/epic03/wrapper.htm?arnumber=6637026.

[19] Robert H. Hadfield. Single-photon detectors for optical quantum information applications. *Nature photonics*, 3(12):696–705, 2009.

[20] Winfried Denk, James H. Strickler, Watt W. Webb, et al. Two-photon laser scanning fluorescence microscopy. *Science*, 248(4951):73–76, 1990.

[21] David E. Kuhl, Jorge R. Barrio, Sung-Cheng Huang, Carl Selin, Robert F. Ackermann, James L. Lear, J.L. Wu, T.H. Lin, and Michael E. Phelps. Quantifying local cerebral blood flow by n-isopropyl-p-[123i] iodoamphetamine (imp) tomography. *Journal of nuclear medicine: official publication, Society of Nuclear Medicine*, 23(3):196–203, 1982.

[22] Anja Wagner, Heiko Mahrholdt, Thomas A Holly, Michael D Elliott, Matthias Regenfus, Michele Parker, Francis J Klocke, Robert O. Bonow, Raymond J Kim, and Robert M. Judd. Contrast-enhanced mri and routine single photon emission computed tomography (spect) perfusion imaging for detection of subendocardial myocardial infarcts: an imaging study. *The Lancet*, 361(9355):374–379, 2003.

[23] Haifeng Wang, Terry B Huff, Daniel A Zweifel, Wei He, Philip S Low, Alexander Wei, and Ji-Xin Cheng. In vitro and in vivo two-photon luminescence imaging of single gold nanorods. *Proceedings of the National Academy of Sciences of the United States of America*, 102(44):15752–15756, 2005.

[24] Jamie Holder, R.W. Atkins, H.M. Badran, G Blaylock, SM Bradbury, J.H. Buckley, K.L. Byrum, D.A. Carter-Lewis, O. Celik, Y.C.K. Chow, et al. The first veritas telescope. *Astroparticle Physics*, 25(6):391–401, 2006.

[25] Photomultiplier tube, 2017. URL https://en.wikipedia.org/wiki/Photomultiplier.

[26] Ugur Akgun. Pmt afterpulse studies.

[27] Microcolimters: Transition edge sensor, 2017. URL http://web.mit.edu/figueroagroup/ucal/ucal_tes/.

[28] Thomas Aref, Per Delsing, Maria K Ekström, Anton Frisk Kockum, Martin V Gustafsson, Göran Johansson, Peter J Leek, Einar Magnusson, and Riccardo Manenti. Superconducting devices in quantum optics. 2016.

[29] Superconducting nanowire single-photon detector, 2017. URL https://en.wikipedia.org/wiki/Superconducting_nanowire_single-photon_detector.

[30] Qi Guo, Hao Li, LiXing You, WeiJun Zhang, Lu Zhang, Zhen Wang, XiaoMing Xie, and Ming Qi. Single photon detector with high polarization sensitivity. *Scientific reports*, 5:9616, 2015.

[31] HEKTOR TAAVI JOSEPH MEIER. *Design, characterization and simulation of avalanche photodiodes*. PhD thesis, ETH ZURICH, 2011.

[32] Bahaa E.A. Saleh, Malvin Carl Teich, and Bahaa E. Saleh. *Fundamentals of photonics*, volume 22. Wiley New York, 1991.

[33] Reverse biased p-n junction diode, 2017. URL http://www.electronics-tutorials.ws/diode/diode_3.html.

[34] Pn junction diode and its characteristics, 2017. URL http://www.circuitstoday.com/pn-junction-diode-characteristics.

[35] S. Cova, M. Ghioni, A. Lacaita, C. Samori, and F. Zappa. Avalanche photodiodes and quenching circuits for single-photon detection. *Applied optics*, 35(12):1956–1976, 1996. ISSN 0003-6935. doi: 10.1364/AO.35.001956.

[36] Thomas Daniel Jennewein. *Quantum communication and teleportation experiments using entangled photon pairs*. na, 2002.

[37] J.F.J. Todd, R.M. Waldren, and R.E. Mather. The quadrupole ion store (quistor) part ix. space-charge and ion stability. a theoretical background and experimental results. *International Journal of Mass Spectrometry and Ion Physics*, 34(3-4):325–349, 1980.

[38] Wikipedia.org: p-n junction, May 2017. URL https://en.wikipedia.org/wiki/P-n_junction.

[39] Lars Vincent van de Wiel Lydersen. *Practical security of quantum cryptography*. PhD thesis, 2011.

[40] R. G. W. Brown, K. D. Ridley, and J. G. Rarity. Characterization of silicon avalanche photodiodes for photon correlation measurements 1: Passive quenching. *Applied Optics*, 25(22):4122, 1986. ISSN 0003-6935. doi: 10.1364/AO.25.004122. URL http://www.opticsinfobase.org/ao/fulltext.cfm?uri=ao-25-22-4122$\delimiter"026E30F$nhttp://www.opticsinfobase.org/abstract.cfm?URI=ao-25-22-4122.

[41] Jie Zhang. Semiconductor optical single-photon detectors. *Department of Electrical and Computer Engineering, University of Rochester, NY*, 14627.

[42] P. Antognetti, S. Cova, and A. Longoni. A study of the operation and performances of an avalanche diode as a single-photon detector. Technical report, 1975.

[43] Robert G. W. Brown, Robin Jones, John G. Rarity, and Kevin D. Ridley. Characterization of silicon avalanche photodiodes for photon correlation measurements. 2: Active quenching. 26(12):2383–2389, 1987.

[44] Nicoletta Dinu. *Instrumentation on Silicon Detectors: from properties characterization to applications*. PhD thesis, Université Paris Sud-Paris XI, 2013.

[45] Thiago Ferreira Da Silva, Guilherme B. Xavier, and Jean Pierre Von Der Weid. Real-time characterization of gated-mode single-photon detectors. *IEEE Journal of Quantum Electronics*, 47(9):1251–1256, 2011. ISSN 00189197. doi: 10.

1109/JQE.2011.2163622. URL http://ieeexplore.ieee.org/lpdocs/epic03/wrapper.htm?arnumber=5975192.

[46] Mark A. Itzler, Mark Entwistle, and Xudong Jiang. High-rate photon counting with Geiger-mode APDs. *IEEE Photonic Society 24th Annual Meeting, PHO 2011*, (April 2016):348–349, 2011. doi: 10.1109/PHO.2011.6110570.

[47] Alessandro Restelli, Joshua C. Bienfang, and Alan L. Migdall. Time-domain measurements of afterpulsing in InGaAs/InP SPAD gated with sub-nanosecond pulses. *Journal of Modern Optics*, 59(August):1–7, 2012. ISSN 0950-0340. doi: 10.1080/09500340.2012.687463.

[48] S. Cova, M. Ghioni, A. Lotito, I. Rech, and F. Zappa. Evolution and prospects for single-photon avalanche diodes and quenching circuits. *Journal of Modern Optics*, 51(9-10):1267–1288, 2004. ISSN 0950-0340. doi: 10.1080/09500340410001670839.

[49] A. Yoshizawa, R. Kaji, and H. Tsuchida. Quantum efficiency evaluation method for gated-mode single-photon detector. *Electronics Letters*, 38(23):1468–1469, 2002.

[50] S. V. Polyakov and A. L. Migdall. High accuracy verification of a correlated-photon-based method for determining photoncounting detection efficiency. *Optics Express*, 15:1390–1407, 2007.

[51] Mario Stipčević and Daniel J. Gauthier. Precise Monte Carlo Simulation of Single-Photon Detectors. 5:1–5, 2014.

[52] Michael Ware, Alan Migdall, Joshua C Bienfang, and Sergey V Polyakov. Calibrating photon-counting detectors to high accuracy: background and deadtime issues. 1(1):1–13, 2006.

[53] M. D. Eisaman, J. Fan, A. Migdall and S. V. Polyakov. Invited Review Article: Single-photon sources and detectors. *Acta Medica Okayama*, 67(4):259–263, 2013. ISSN 0386300X. doi: 10.1063/1.3610677.

[54] H. T. Yen, S. D. Lin, and C. M. Tsai. A simple method to characterize the afterpulsing effect in single photon avalanche photodiode. *Journal of Applied Physics*, 104(5):1–5, 2008. ISSN 00218979. doi: 10.1063/1.2968434.

[55] Boris Korzh, Tommaso Lunghi, Kateryna Kuzmenko, Gianluca Boso, and Hugo Zbinden. Afterpulsing studies of low-noise InGaAs/InP single-photon negative-feedback avalanche diodes. *Journal of Modern Optics*, (July):1–7, 2015. ISSN 0950-0340. doi: 10.1080/09500340.2015.1024294. URL http://www.tandfonline.com/doi/abs/10.1080/09500340.2015.1024294.

[56] Viacheslav Burenkov. Security Issues of Quantum Cryptographic Systems with Imperfect Detectors. 2015. URL

https://tspace.library.utoronto.ca/bitstream/1807/69219/3/Burenkov{_}Viacheslav{_}V{_}201506{_}PhD{_}thesis.pdf.

[57] M. Höbel and J. Ricka. Dead-time and afterpulsing correction in multiphoton timing with nonideal detectors. *Review of Scientific Instruments*, 65(7):2326–2336, 1994. ISSN 00346748. doi: 10.1063/1.1144684.

[58] Sebastien Sauge, Lars Lydersen, Andrey Anisimov, Johannes Skaar, and Vadim Makarov. Controlling an actively-quenched single photon detector with bright light. *Optics Express*, 19(23):23590–23600, 2011.

[59] Lars Lydersen, Carlos Wiechers, Christoffer Wittmann, Dominique Elser, Johannes Skaar, and Vadim Makarov. Thermal blinding of gated detectors in quantum cryptography. *Optics express*, 18(26):27938–27954, 2010.

[60] Charles H. Bennett and Gilles Brassard. Quantum cryptography: Public key distribution and con tos5. 1984.

[61] Won-Young Hwang. Quantum key distribution with high loss: toward global secure communication. *Physical Review Letters*, 91(5):057901, 2003.

[62] Xiang-Bin Wang. Beating the photon-number-splitting attack in practical quantum cryptography. *Physical review letters*, 94(23):230503, 2005.

[63] Joshua A Slater, Cyril Branciard, Nicolas Brunner, and Wolfgang Tittel. Device-dependent and device-independent quantum key distribution without a shared reference frame. *New Journal of Physics*, 16(4):043002, 2014.